






**Inhomogeneous superconductivity in  $\text{Lu}_x\text{Zr}_{1-x}\text{B}_{12}$  dodecaborides with dynamic charge stripes**

A. Azarevich <sup>1</sup>, A. Bogach,<sup>1</sup> V. Glushkov <sup>1</sup>, S. Demishev,<sup>1</sup> A. Khoroshilov,<sup>1</sup> K. Krasikov,<sup>1</sup> V. Voronov,<sup>1</sup>  
N. Shitsevalova,<sup>2</sup> V. Filipov,<sup>2</sup> S. Gabáni <sup>3</sup>, K. Flachbart <sup>3</sup>, A. Kuznetsov <sup>4</sup>, S. Gavrilkin,<sup>5</sup>

K. Mitsen <sup>5</sup>, S. J. Blundell,<sup>6</sup> and N. E. Sluchanko <sup>1</sup>

<sup>1</sup>*Prokhorov General Physics Institute of the Russian Academy of Sciences, Vavilov str. 38, Moscow 119991, Russia*

<sup>2</sup>*Frantsevich Institute for Problems of Materials Science, National Academy of Sciences of Ukraine, 03680 Kyiv, Ukraine*

<sup>3</sup>*Institute of Experimental Physics of the Slovak Academy of Sciences, Watsonova 47, 04001 Košice, Slovakia*

<sup>4</sup>*National Research Nuclear University MEPhI, 31, Kashirskoe Shosse, 115409 Moscow, Russia*

<sup>5</sup>*Lebedev Physical Institute of the Russian Academy of Sciences, 53 Leninskiy Avenue, 119991 Moscow, Russia*

<sup>6</sup>*Department of Physics, University of Oxford, Clarendon Laboratory, Parks Road, Oxford OX1 3PU, United Kingdom*



(Received 21 December 2020; revised 1 March 2021; accepted 9 March 2021; published 25 March 2021)

We have studied the normal and superconductive state characteristics (resistivity, Hall coefficient, heat capacity, and magnetization) of model strongly correlated electronic systems  $\text{Lu}_x\text{Zr}_{1-x}\text{B}_{12}$  with cooperative Jahn-Teller instability of the boron rigid cage and with dynamic charge stripes. It was found that these metals are *s*-wave dirty limit superconductors with a small mean free path of charge carriers  $l = 5\text{--}140$  Å and with a Cooper pair size changing nonmonotonously in the range 450–4000 Å. The parent  $\text{ZrB}_{12}$  and  $\text{LuB}_{12}$  borides are type-I superconductors, and Zr to Lu substitution induces a type-I to type-II phase transition providing a variation of the Ginzburg-Landau-Maki parameter in the limits  $0.65 \leq \kappa_{1,2} \leq 6$ . We argue in favor of the two-band scenario of superconductivity in  $\text{Lu}_x\text{Zr}_{1-x}\text{B}_{12}$  with gap values  $\Delta_1 \sim 14$  K and  $\Delta_2 \sim 6\text{--}8$  K, with pairing corresponding to strong coupling limit ( $\lambda_{e\text{-ph}} \sim 1$ ) in the upper band, and to weak coupling ( $\lambda_{e\text{-ph}} \sim 0.1\text{--}0.4$ ) in the lower one. A pseudogap  $\Delta_{\text{ps-gap}} \sim 60\text{--}110$  K is observed in  $\text{Lu}_x\text{Zr}_{1-x}\text{B}_{12}$  above  $T_c$ . We discuss also the possibility of anisotropic single-band superconductivity with stripe-induced both pair breaking and anisotropy, and analyze the origin of a unique enhanced surface superconductivity detected in these model compounds.

DOI: [10.1103/PhysRevB.103.104515](https://doi.org/10.1103/PhysRevB.103.104515)

## I. INTRODUCTION

During the last 35 years studies of high temperature superconductivity (HTSC) were developed on cuprates (see, for example, [1–7]), Fe-based pnictides and chalcogenides [8–17], and  $\text{MgB}_2$  [18–23] to understand the mechanisms at work. In these unconventional and conventional HTSC a lot of unusual phenomena have been found including charge and spin stripes [2–4,7,12], electron nematic effect [2,6], pseudogap and strange metal phase [2–6,12–14], multiband superconductivity of different type [14–24], etc. It was suggested that at least some of these anomalies are closely related to the mechanism underlying the superconductivity enhancement [2–6,12–14]. It is believed now that  $\text{MgB}_2$  clearly belongs to a different class than unconventional HTSCs, being a phonon-driven superconductor, while true, high temperature superconductivity both in cuprates and Fe-based compounds is a strong correlation phenomenon [2–6,14]. At the same time, however, regardless of that how unique the cuprates may be, these features are not prerequisites for nonphonon high temperature superconductivity [14]. Thus, it is believed at present that the interplay of different simultaneously active charge, spin, lattice, and orbital interactions plays a key role not only in the formation of a rich variety of phases in phase diagrams of strongly correlated electron systems (SCES), but that they also provide the essential ingredients of HTSC [2–6,12–14,25].

The discovery of superconductivity at  $T_c \approx 39$  K in  $\text{MgB}_2$  [18] stimulated a significant interest in the studies of a wide class of the rare-earth and transition-metal borides. Among them, in the family of high borides  $\text{RB}_{12}$ , zirconium dodecaboride is supposed to be a BCS superconductor with the highest  $T_c \approx 6$  K [26,27]. An important feature established for  $\text{ZrB}_{12}$  is the key role in the formation of Cooper pairs coming from quasilocal vibrations (rattling modes) involving  $\text{Zr}^{4+}$  ions located within truncated  $\text{B}_{24}$  octahedrons in the  $\text{UB}_{12}$ -type fcc crystal structure [26–29] (see Fig. 1). In studies of the Einstein phonon mediated superconductivity in  $\text{ZrB}_{12}$ , the authors of [26–33] argue that *s*-wave pairing is characteristic for this compound, and that the Ginzburg-Landau-Maki (GLM) parameter  $\kappa$  is located in the nearest vicinity of the threshold value  $\kappa_c = 1/\sqrt{2}$ . Moreover, a crossover from type-I to type-II/1 superconductivity with temperature lowering was deduced in [27] from heat capacity and magnetization measurements [see inset in Fig. 3(b) below]. In contrast, in [34] the superconductivity in  $\text{ZrB}_{12}$  was interpreted in terms of *d*-wave pairing and a two-gap type-II regime was identified. Additionally, a large size pseudogap ( $\Delta_{\text{ps-gap}} \sim 7.3$  meV) has been detected employing high resolution photoemission spectroscopy in  $\text{ZrB}_{12}$  above  $T_c$ , and proximity to the quantum fluctuation regime was predicted from the *ab initio* band structure calculations [35]. Thus, a similarity with cuprate HTSC has led to a revival in interest in this low temperature superconductor.

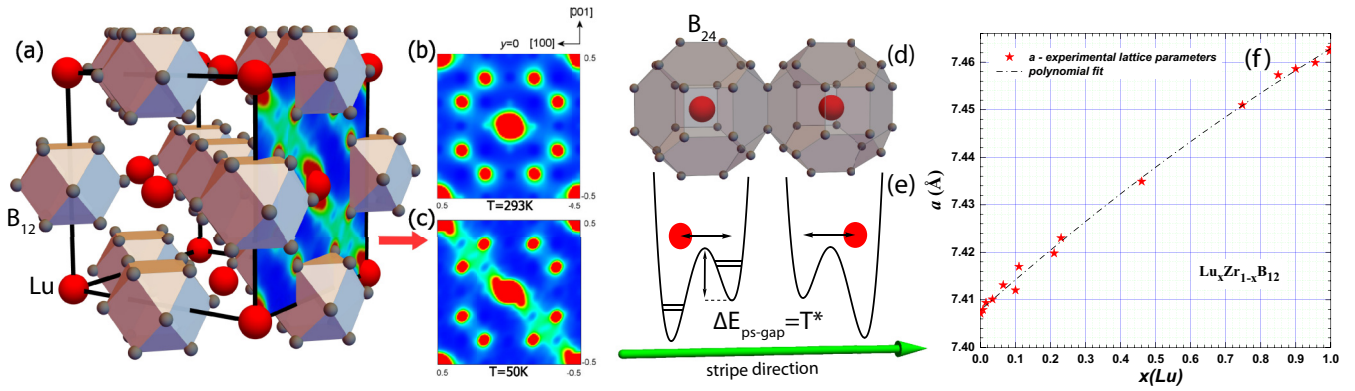


FIG. 1. (a) Crystal structure of  $RB_{12}$ . The color plane shows the distribution of the electron density in dynamic charge stripes (green bands) along with  $[110]$  direction as observed in [43] at  $T = 50$  K. (b) and (c) The electron density changes between  $T = 293$  K (b) and 50 K (c) as deduced from  $x$ -ray diffraction experiment by the maximal entropy method [43]. (d) Fragment of  $RB_{12}$  crystal structure composed from two truncated cubo-octahedrons  $B_{24}$  centered by Lu/Zr ions. (e) Schematic view of two double-well potentials in vicinity of Lu/Zr ions with oscillations of metallic ions from their central positions inside the  $B_{24}$  cubo-octahedra. The barrier height in the double-well potential (the pseudogap) is about equal to the cage-glass transition temperature  $\Delta E_{ps-gap} \cong T^*$ . (f) The lattice constant  $a(x)$  variation in  $Lu_xZr_{1-x}B_{12}$ .

In the case of  $RB_{12}$  the replacement of heavy nonmagnetic ions from Zr by Lu produces an approximately 15-fold reduction in superconductivity [28,33,36,37] ( $T_c \approx 0.4$  K for  $LuB_{12}$ ), and the origin of this  $T_c$  suppression is not cleared up to now for these two compounds with a similar conduction band and the same crystalline  $UB_{12}$ -type structure [Fig. 1(a)]. Indeed, inelastic neutron scattering studies of the phonon spectra in  $LuB_{12}$  and  $ZrB_{12}$  have detected noticeable but not dramatic changes in the position of the almost dispersionless quasilocal mode (15 and 17.5 meV, correspondingly [29]), which was proposed to be responsible for Cooper pairing. Only a moderate difference in electron density of states (DOS) of these two compounds is caused by filling the wide enough conduction band ( $\sim 1.6$ – $2$  eV [28,38,39]) when the  $Lu^{3+}$  ion is changed to  $Zr^{4+}$  in the  $RB_{12}$  unit cell, resulting in elevation by about 0.3–0.4 eV of the Fermi level  $E_F$  for  $ZrB_{12}$  in comparison with  $LuB_{12}$  [35,40]. An evidence for the formation of nodes in the superconducting gap of Zr-rich  $Lu_xZr_{1-x}B_{12}$  dodecaborides was found in [41] and then a  $s + d$ - to  $s$ -wave crossover was observed using these  $\mu$ SR measurements. The authors of [41] note that the unusual *transition from nodal to gapped superconductivity* is similar to that observed in iron pnictide superconductors.

Recently it was detected that a Jahn-Teller instability of the rigid boron cage develops in  $LuB_{12}$  and is accompanied by formation of *dynamic charge stripes* [see Figs. 1(a)–1(c)] both in the nonmagnetic reference compound as well as in rare-earth dodecaborides with magnetic ions [42–46]. Besides, an order-disorder phase transition was found in  $LuB_{12}$  at  $T^* \sim 60$  K [47] and below  $T^*$  an infinite cluster in the filamentary structure of stripes appears in the cage-glass state with random displacement of R ions from central positions in  $B_{24}$  cubo-octahedra [44] [see Figs. 1(d) and 1(e)]. Thus, taking into account that the essential ingredients of HTSC (stripes, pseudogap,  $s + d$ -wave superconductivity) are observed also in conventional  $Lu_xZr_{1-x}B_{12}$  superconductors, it is promising to study in detail both the normal and superconducting state characteristics of these nonequilibrium dodeca-

borides to look for commonalities which may be important for HTSC.

Here we probed the evolution of superconducting and normal state parameters for substitutional solid solutions  $Lu_xZr_{1-x}B_{12}$  employing resistivity, Hall effect, heat capacity, and magnetization measurements. It will be shown below that the purest parent  $ZrB_{12}$  and  $LuB_{12}$  compounds are inhomogeneous type-I superconductors with dynamic charge stripes. The nonmagnetic Lu impurity substitution then induces a type-I to type-II transition in  $Lu_xZr_{1-x}B_{12}$  which is accompanied by  $T_c$  lowering and nonmonotonous changes in the coherence length  $\xi = 450$ – $4000$  Å exhibiting a minimum near the Lu percolation threshold  $x_c \sim 0.23$ . We discuss two alternative scenarios of superconductivity in the dirty limit: (i) two bands with the  $s$ -wave pairing and (ii) single-band  $s$ -wave anisotropic superconductivity in the presence of a strong stripe induced pair-breaking mechanism along  $\langle 110 \rangle$  direction. A pseudogap state with  $\Delta_{ps-gap} = 60$ – $110$  K is detected above  $T_c$  in all studied  $Lu_xZr_{1-x}B_{12}$  dodecaborides, but the pseudogap  $\Delta_{ps-gap}(x)$  evolution is not directly related to  $T_c$ .

## II. EXPERIMENTAL DETAILS

The high quality single crystals of  $Lu_xZr_{1-x}B_{12}$  solid solutions were grown by crucible-free inductive floating zone technique in the inert gas atmosphere (see [48] for more detail). The quality and single phase of crystals were controlled by  $x$ -ray diffraction. In order to control the composition of samples we used additional optical emission spectral analysis and microanalysis [48]. The obtained values of lattice constant  $a(x)$  are shown in Fig. 1(f) in combination with the schematic view of the  $UB_{12}$ -type crystal structure [Fig. 1(a)] and the location of dynamic charge stripes detected in  $LuB_{12}$  single crystals (Figs. 1(b) and 1(c) [43]). The heat capacity was measured using a Quantum Design PPM-9 installation in the Shared Facility Centre of Lebedev Physical Institute of RAS in the temperature range 0.3–300 K and in magnetic fields up to 9 T. Field and temperature dependencies of

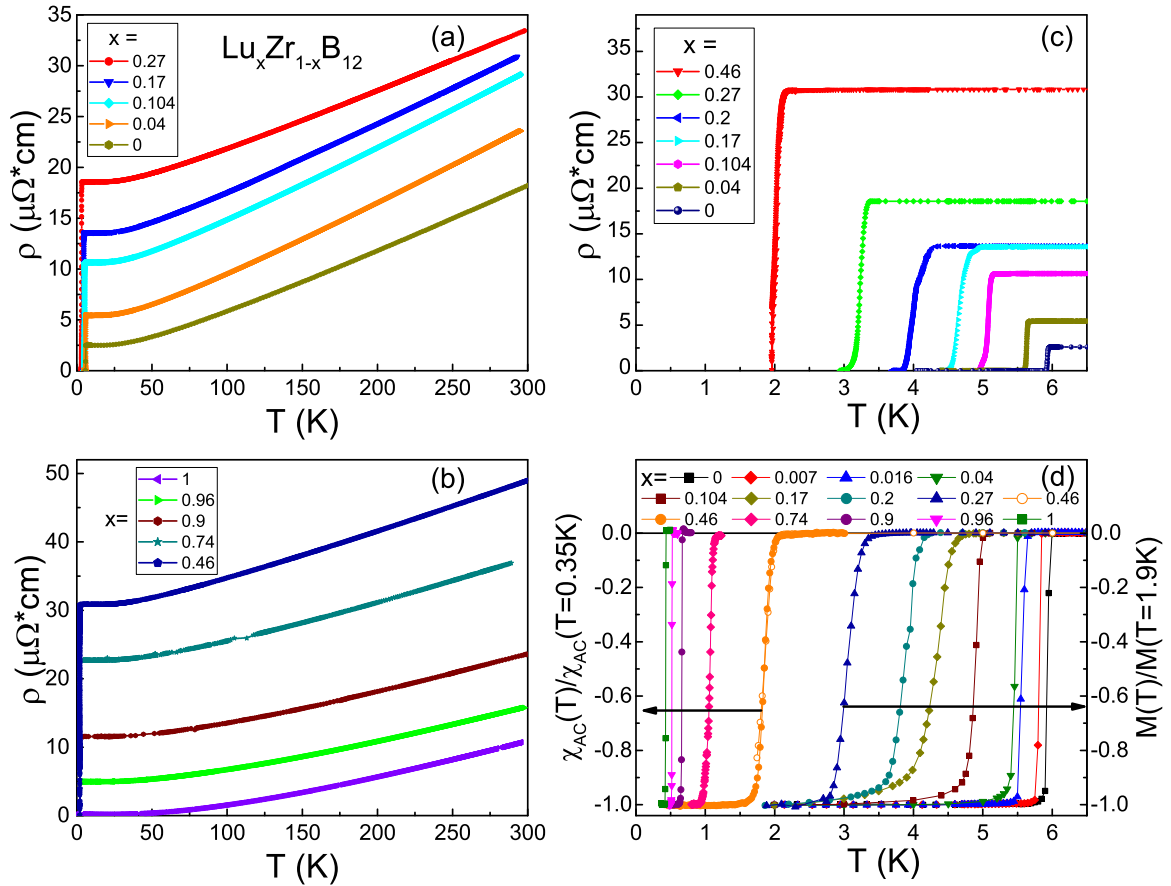


FIG. 2. (a) and (b) The temperature dependencies of resistivity  $\rho(T)$  of several  $\text{Lu}_x\text{Zr}_{1-x}\text{B}_{12}$  crystals. (c) The large scale of  $\rho(T)$  near  $T_c$  demonstrates the superconducting transition for Zr-rich samples of  $\text{Lu}_x\text{Zr}_{1-x}\text{B}_{12}$ . (d) The diamagnetic response measured in field cooled (1–6 Oe) MPMS experiments for  $x < 0.46$  Lu composition and in AC magnetic susceptibility studies in  $^3\text{He}$ - $^4\text{He}$  minifridge.

magnetization were recorded by a Quantum Design MPMS-5. To measure the magnetic characteristics down to very low temperatures ( $\sim 50$  mK) an original AC susceptometer based in a dilution  $^3\text{He}$ - $^4\text{He}$  minirefrigerator was applied [49]. For measurements of resistivity and Hall effect we used an original setup described in [50].

### III. EXPERIMENTAL RESULTS AND DATA ANALYSIS

#### A. Resistivity

Figures 2(a) and 2(b) show the temperature dependencies of resistivity  $\rho(T)$  of several studied  $\text{Lu}_x\text{Zr}_{1-x}\text{B}_{12}$  crystals. The  $\rho(T)$  curves exhibit a typical metallic behavior with an about linear temperature dependence  $\rho = \rho_0 + \alpha T$  in the range  $T > 80$  K and a rather small residual resistivity ratio  $\rho(300\text{K})/\rho_0 = 1.8\text{--}20$ . The large scale plot on Fig. 2(c) demonstrates the superconducting transitions of Zr-rich  $\text{Lu}_x\text{Zr}_{1-x}\text{B}_{12}$  samples. For  $\text{Lu}_x\text{Zr}_{1-x}\text{B}_{12}$  single crystals with  $x \neq 0$  we observed a wide enough resistivity transition with a width  $\Delta T_c^{(\rho)} \sim 0.1\text{--}0.4$  K as well as a nonmonotonous  $\rho(T)$  behavior near  $T_c$  [Fig. 2(c)]. Both the residual resistivity  $\rho_0(x)$  and the slope  $\alpha(x)$  change nonmonotonously with a maximum near  $x \sim 0.5$ , and an additional singularity is observed in vicinity of the Lu percolation threshold  $x_c \sim 0.23$  [Fig. 3(a)]. A detailed analysis of the resistivity temperature dependencies, similar to the one presented for

$\text{LuB}_{12}$  in [44], is outside the scope of this paper and will be published elsewhere. Note that the anomaly at  $x_c$  may be attributed to pinning of the dynamic charge stripes on Lu impurities leading to formation of an infinite cluster (filamentary structure of fluctuating electron density) near the percolation threshold.

#### B. Magnetoresistance and Hall effect

Field and temperature dependencies of magnetoresistance (MR)  $\Delta\rho/\rho(H, T)$  and Hall coefficient  $R_H(H, T)$  have been studied here for a number of  $\text{Lu}_x\text{Zr}_{1-x}\text{B}_{12}$  crystals (see, for example, Figs. 4(a)–4(c) and Figs. S8 and S9 in [48]). A quadratic MR behavior  $\Delta\rho/\rho \approx \mu_D^2 H^2$  was found and dependencies of the drift mobility of charge carriers  $\mu_D(T)$  [Fig. 4(d)] and  $\mu_D(x)$  [Fig. 4(e)] have been deduced from the data obtained. It is shown in Fig. 4(c) that in solid solutions  $\text{Lu}_x\text{Zr}_{1-x}\text{B}_{12}$  the Hall coefficient  $R_H(H, T = 4.2\text{K})$  is a practically field independent parameter and Hall mobility  $\mu_H = R_H/\rho$  temperature and concentration changes  $\mu_H(T)$  and  $\mu_H(x, T = 4.2\text{K})$  have been estimated [see, e.g., Figs. 4(d) and 4(e), correspondingly]. The Hall factor  $\mu_H(x)/\mu_D(x)$  varies in the range 0.45–0.9 and taking the effective mass  $m^* \sim 0.7m_0$  [51–53] we estimate also the average relaxation time of charge carriers  $\tau(x)$  [Fig. 4(e)]. It is worth noting that the small enough magnitude of the Hall and drift

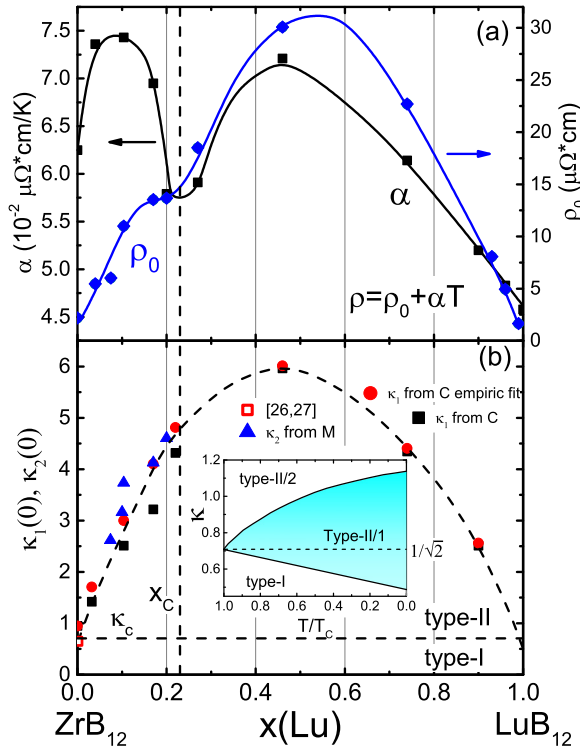


FIG. 3. (a) Residual resistivity  $\rho_0(x)$  and slop  $\alpha(x)$  of the  $\rho(T, x) = \rho_0(x) + \alpha(x)T$  dependence as estimated in temperature range 80–300 K. (b) Concentration dependence of the GLM parameters  $\kappa_1(0)$  and  $\kappa_2(0)$  in  $\text{Lu}_x\text{Zr}_{1-x}\text{B}_{12}$ . Inset in (b) shows a phase diagram fragment in the superconducting state of  $\text{ZrB}_{12}$  where type-I, type-II/1, and type-II/2 phases are shown (see also text). Vertical and horizontal dashed lines show the Lu percolation threshold at  $x_c \sim 0.23$  and the critical value  $\kappa_c = 1/\sqrt{2}$  on the boundary of type-I and type-II superconductivity, correspondingly.

mobility 10–300  $\text{cm}^2/(\text{V s})$  (low magnetic field regime  $\omega_c \tau \ll 1$ , where  $\omega_c$  is the cyclotron frequency) is controlled both by the substitutional disorder and random displacement of heavy Zr/Lu ions from the central positions in the B<sub>24</sub> cuboctahedrons in  $\text{Lu}_x\text{Zr}_{1-x}\text{B}_{12}$  solid solutions reaching the minimum values near  $x \sim 0.5$  [Fig. 4(e)].

### C. Specific heat

The heat capacity temperature dependencies  $C(T)$  of several investigated  $\text{Lu}_x\text{Zr}_{1-x}\text{B}_{12}$  single crystals are shown in Fig. 5(a). Figures 5(b) and 5(c) highlight the zero-field normalized heat capacity behavior in the superconducting state. In addition, Fig. 5(a) shows also the  $C(T)/T = f(T^2)$  curves measured in a magnetic field of about 1 kOe in which the superconductivity of studied compounds is completely suppressed. The plot is commonly used to determine the Sommerfeld coefficient  $\gamma$  of the electronic heat capacity. As can be seen in Fig. 5(a), a gradual diminution of heat capacity at temperatures between 300 and 50 K is followed by a sharp almost steplike decrease with a typical Einstein-type  $C(T)$  dependence below 40 K. It is worth noting that although in the normal state at  $T > 30$  K the  $C(T)$  curves of all  $\text{Lu}_x\text{Zr}_{1-x}\text{B}_{12}$  samples are almost identical in the double logarithmic plot

used in Fig. 5(a), the position of the steplike  $C(T)$  anomaly shifts up along the  $T$  axis when the concentration  $x$  decreases (see, e.g., Fig. S10 [48]).

A comparative analysis of contributions to specific heat in the normal state of  $\text{Lu}_x\text{Zr}_{1-x}\text{B}_{12}$  was carried out in the framework of the approach developed for cage-glass systems in [33,44,47]. The Debye temperatures  $\theta_D(\text{Lu}^N\text{B}_{12}) = 1190$  K and  $\theta_D(\text{Zr}^N\text{B}_{12}) = 1500$  K were used to estimate the contribution from the boron sublattice component  $C_{\text{ph}}$  [28,33,44,47,54]. After elimination both the electron heat capacity  $C_{\text{el}} = \gamma T$  and Debye component  $C_D$  the rest  $C_{\text{exp}} - C_{\text{el}} - C_D$  was approximated by a sum of Einstein oscillators  $C_E$  attributed to Zr and Lu vibrations in oversized B<sub>24</sub> octahedron cages,

$$\frac{C_E}{T^3} = \frac{3R}{\theta_E^3} \left( \frac{\theta_E}{T} \right)^5 \frac{e^{-\theta_E/T}}{(1 - e^{-\theta_E/T})^2} \quad (1)$$

and Schottky type contributions

$$C_{\text{Schi}} = RN_i g_{0i} g_{1i} \left( \frac{\Delta E_i}{k_B T} \right)^2 \frac{e^{\frac{\Delta E_i}{k_B T}}}{(g_{0i} e^{\frac{\Delta E_i}{k_B T}} + g_{1i})^2} \quad (2)$$

( $R$  denotes the gas constant,  $\theta_E$  denotes Einstein temperature,  $g_{0i}$  and  $g_{1i}$  are the degeneracies,  $i = 1, 2$ , and  $\Delta E_i$  are the splitting energies) provided by  $N_i$  two-level systems (TLS) arranged in double-well potentials (DWP) in the vicinity of the randomly distributed Zr/Lu ions [see Fig. 1(e)]. It was found in [47] that the TLS are created resulting from displacement of these heavy ions from the central positions inside B<sub>24</sub> cavities in the disordered cage-glass phase of the RB<sub>12</sub> compounds [47,55,56]. The examples of the  $\text{Lu}_x\text{Zr}_{1-x}\text{B}_{12}$  data analysis are presented in Fig. S11 in [48]. A detailed analysis of the specific heat temperature dependencies is outside the scope of this article and will be published elsewhere. It is worth noting here that the splitting energy  $\Delta E_2$  for TLS<sub>2</sub> in Eq. (2), or, in another words, the barrier in the double-well potential in the vicinity of heavy ions [Fig. 1(e)] should be attributed to the pseudogap  $\Delta_{\text{ps-gap}} = \Delta E_2 \cong T^*$ , and, hence, when the temperature decreases below  $T^*$  the freezing in potential minima of DWP is the main factor which is responsible for the local disorder in the position of Zr/Lu ions. As detected in the  $\text{Lu}_x\text{Zr}_{1-x}\text{B}_{12}$  family the pseudogap changes  $\Delta_{\text{ps-gap}}(x)$  are shown in Fig. 6(a).

The results of heat capacity measurements at low temperatures and in small magnetic fields which just destroy superconductivity are presented in Fig. 7. For comparison, these curves are shown for samples  $x = 0.1, 0.46$ , and  $0.74$  with a significantly different  $T_c$  [see Figs. 7(a), 7(b), and 7(c), respectively] in coordinates  $C(T, H_0)/T$  vs  $T$  (see also Fig. S12 in [48]). Note that the superconducting transition temperature  $T_c(x)$  [Fig. 6(a)] deduced from the heat capacity data are similar to those obtained both from resistivity [Fig. 2(c)] and field-cooled ( $H = 1\text{--}6$  Oe) magnetization curves [see Fig. 2(d)]. Apart from  $T_c(x)$  changes in  $\text{Lu}_x\text{Zr}_{1-x}\text{B}_{12}$  there are also differences related to both lowering of the jump amplitude  $\Delta C$  near  $T_c$  and the broadening of this anomaly (see Fig. S13 in [48]). For all samples except the one with  $x = 0.03$ , the linear dependencies in the upper-left part of Fig. 5(a) allow us to estimate the  $\gamma(x)$  values [see Fig. 8(a)], whereas

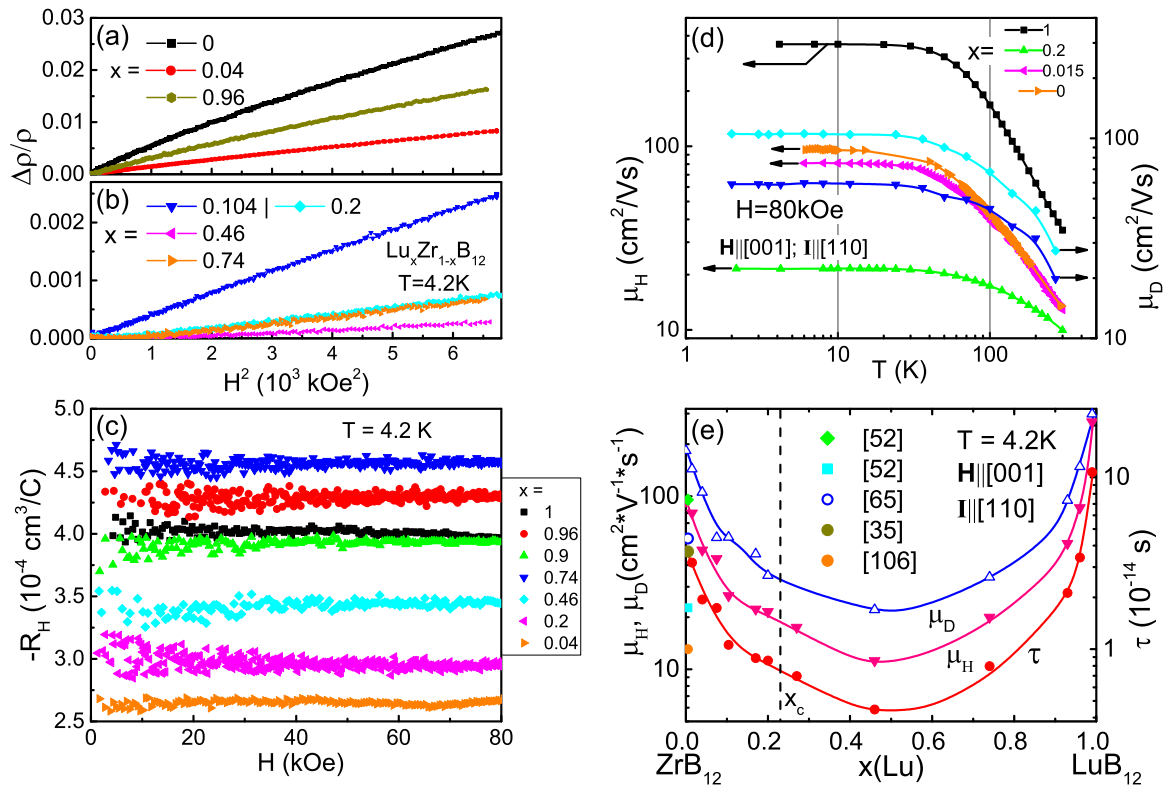


FIG. 4. Field dependencies of magnetoresistance  $\Delta\rho/\rho(H, T = 4.2 \text{ K})$  [(a) and (b)] and Hall coefficient  $R_H(H, T = 4.2 \text{ K})$  (c) measured in  $\text{Lu}_x\text{Zr}_{1-x}\text{B}_{12}$ . (d) Temperature dependencies of drift  $\mu_D(T)$  and Hall  $\mu_H = R_H/\rho(T)$  mobilities of charge carriers measured for several  $\text{Lu}_x\text{Zr}_{1-x}\text{B}_{12}$  crystals at  $H = 80 \text{ kOe}$ . (e) Concentration dependencies of drift  $\mu_D(x, T = 4.2 \text{ K})$  and Hall  $\mu_H(x, T = 4.2 \text{ K})$  mobilities and the average relaxation time  $\tau(x)$  (see text for more detail). Vertical dashed line shows the Lu percolation threshold at  $x_c \sim 0.23$ .

the low temperature specific heat of the  $x = 0.03$  sample is obviously influenced by a moderate additional magnetic contribution.

It should be mentioned that magnetic and nonmagnetic  $\text{Lu}_x\text{Zr}_{1-x}\text{B}_{12}$  samples have been found previously [37,41,57] depending on both the crystal growth conditions and the

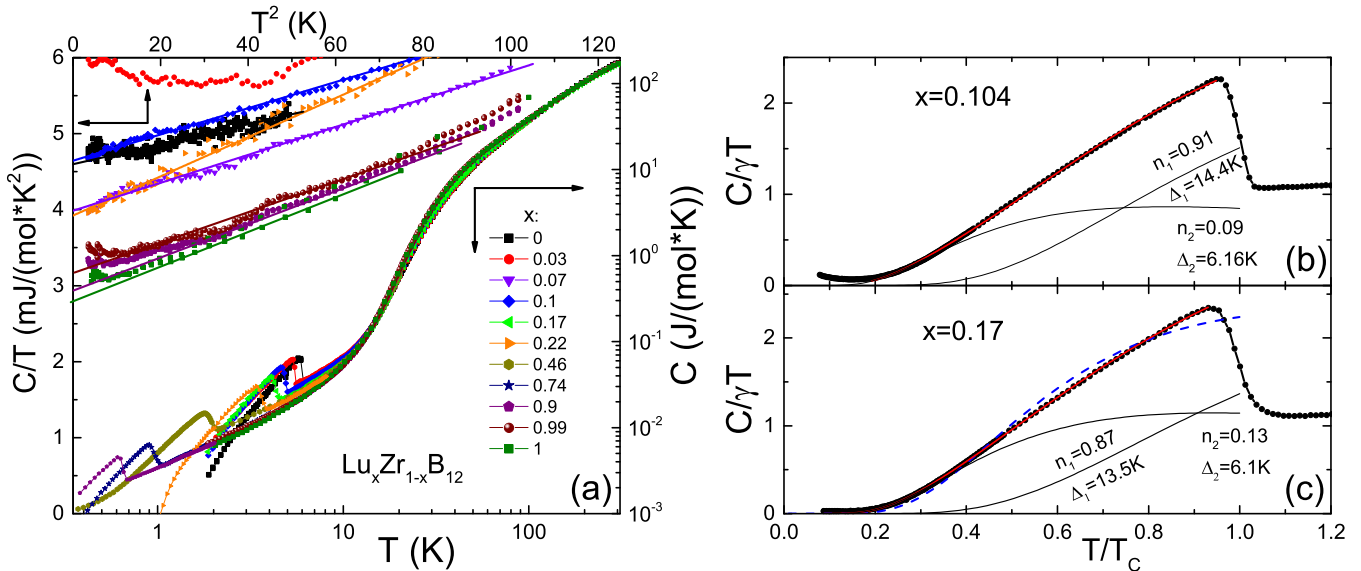


FIG. 5. (a) Zero field heat capacity temperature dependencies  $C(T)$  (right bottom) and corresponding  $C(T)/T = f(T^2)$  curves measured in magnetic field of about 1 kOe which destroys superconductivity (left top) of a number of investigated  $\text{Lu}_x\text{Zr}_{1-x}\text{B}_{12}$  single crystals. (b) and (c) Highlight the zero-field normalized heat capacity behavior in the superconducting state of (b)  $\text{Lu}_{0.104}\text{Zr}_{0.896}\text{B}_{12}$  and (c)  $\text{Lu}_{0.17}\text{Zr}_{0.83}\text{B}_{12}$ . Thick solid and dashed lines show the fits using the two-band and single-band  $\alpha$  models (see text), correspondingly. Thin lines present the smaller-gap and larger-gap components.

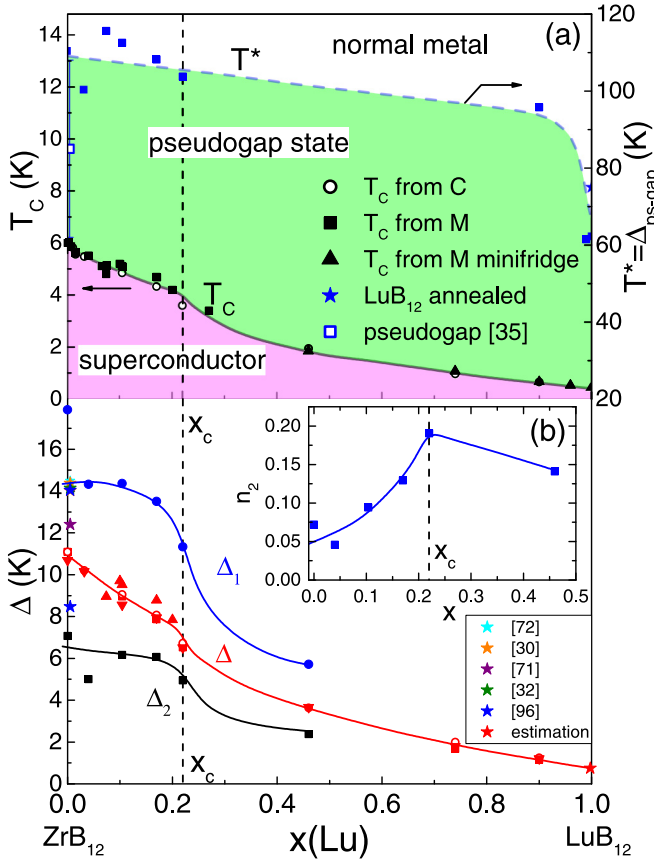


FIG. 6. (a) Pseudogap  $\Delta_{\text{ps-gap}}(x) \cong T^*(x)$  and superconducting transition temperature  $T_c(x)$  changes in  $\text{Lu}_x\text{Zr}_{1-x}\text{B}_{12}$  solid solutions. The color areas show the pseudogap (green) and superconducting (pink) states. (b) Concentration dependencies of the single-band average superconducting gap  $\Delta(0)$  [see Eq. (10)] and the two-band gaps  $\Delta_1(0)$  and  $\Delta_2(0)$  derived within the  $\alpha$  model in  $\text{Lu}_x\text{Zr}_{1-x}\text{B}_{12}$ . Inset presents the  $x$  dependence of the relative weight  $n_2(x)$  of the smaller-gap component.

location of Lu ions in crystals. Moreover, the formation of magnetic nanodomains near the pairs of randomly distributed Lu ions in the  $\text{Lu}_x\text{Zr}_{1-x}\text{B}_{12}$  solid solutions was concluded to be responsible for the low temperature magnetic component of the heat capacity [41,57]. It is well known at present that any magnetic defects, clusters, and spin glass

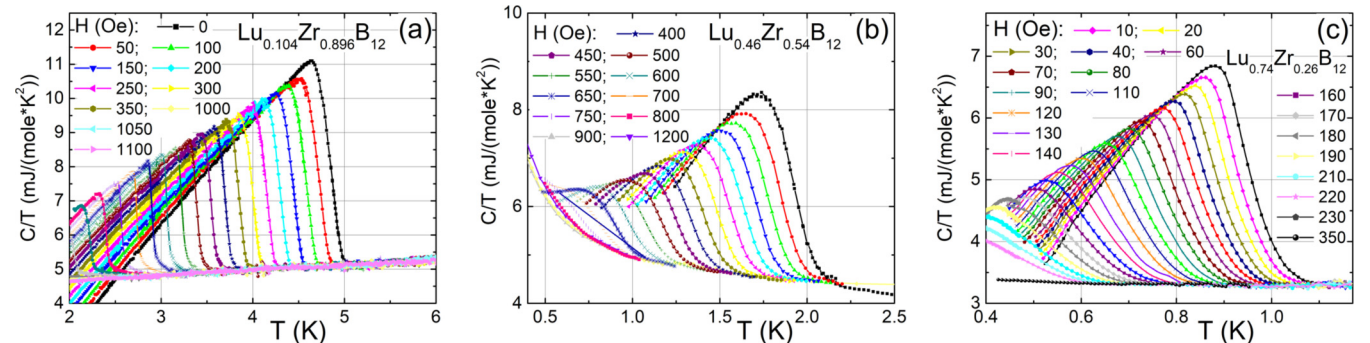


FIG. 7. Low temperature heat capacity dependencies  $C(T, H_0)/T$  of (a)  $\text{Lu}_{0.104}\text{Zr}_{0.896}\text{B}_{12}$ , (b)  $\text{Lu}_{0.46}\text{Zr}_{0.54}\text{B}_{12}$ , and (c)  $\text{Lu}_{0.74}\text{Zr}_{0.26}\text{B}_{12}$  in small magnetic fields which destroy the superconductivity.

behavior can result into a specific heat enhancement [58] and lead in some cases to a false indication of heavy fermion behavior [59,60]. In such cases a detailed investigation of magnetic field changes of the low temperature heat capacity can help to identify the nature of the enhancement. For this reason we have carried out field dependent heat capacity measurements of the magnetic crystal  $x = 0.03$  to separate the electronic and magnetic contributions. The obtained magnetic component which shifts up along the temperature axis when the magnetic field increases, prevails essentially the electronic Sommerfeld term [ $\gamma(x = 0.03) \sim 4.3 \text{ mJ}/(\text{mol K}^2)$ ] and demonstrates a moderate increase in external magnetic field (see Fig. S14 in [48] for more details).

The specific heat results obtained in the normal and superconducting states (Figs. 5, 7, and S12) were used to determine the thermodynamic critical field  $H_{\text{cm}}(T)$  within the framework of standard relations

$$-1/2\mu_0 V H_{\text{cm}}^2(T) = \Delta F(T) = \Delta U(T) - T \Delta S(T), \quad (3)$$

$$\Delta U(T) = \int [C_s(T') - C_n(T')] dT', \quad (4)$$

$$\Delta S(T) = \int dT' [C_s(T') - C_n(T')]/T', \quad (5)$$

where  $F$  and  $U$  denote the free and internal energies,  $S$  is the entropy,  $V$  is the molar volume, and the indices  $n$  and  $s$  correspond to characteristics of the normal and superconducting phases of  $\text{Lu}_x\text{Zr}_{1-x}\text{B}_{12}$ . The integration was carried out in the temperature range from  $T$  to  $T_c$ . Before integration the specific heat data in the normal and superconducting states were approximated by polynomials of the fourth order. Figure 9 shows the dependencies of the thermodynamic  $H_{\text{cm}}(T)$  and upper  $H_{c2}(T)$  critical fields, respectively, resulting from the heat capacity analysis of studied crystals. Figure 10(a) presents both the  $H_{\text{cm}}(0)$  values obtained by extrapolation of  $H_{\text{cm}}(T)$  curves in the framework of the standard Bardeen-Cooper-Schiffer (BCS) relation [61]

$$\begin{aligned} H_{\text{cm}}(T)/H_{\text{cm}}(0) = & 1.7367(1 - T/T_c)[1 - 0.327(1 - T/T_c) \\ & - 0.0949(1 - T/T_c)^2] \end{aligned} \quad (6)$$

and  $H_{c2}(0)$  magnitudes defined within the framework of formula used in [62],

$$H_{c2}(0) = -0.69T_c(dH_{c2}/dT)_{T=T_c} \quad (7)$$

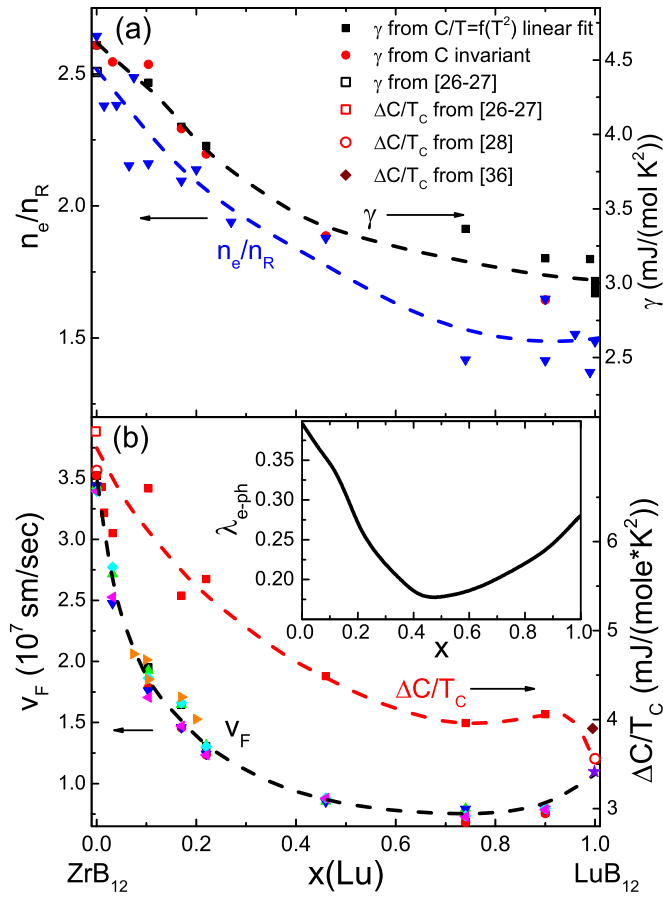


FIG. 8. Lu content dependencies of (a) the Sommerfeld coefficient  $\gamma(x)$  and the normalized concentration of charge carriers  $n_e/n_R(x) = 1/(R_H en_R)$ , and (b) the jump of heat capacity  $\Delta C/T_c(x)$  and the average Fermi velocity  $v_F(x)$ . Inset in (b) shows changes of the electron-phonon interaction constant  $\lambda_{e\text{-ph}}(x)$  in  $\text{Lu}_x\text{Zr}_{1-x}\text{B}_{12}$  (see text).

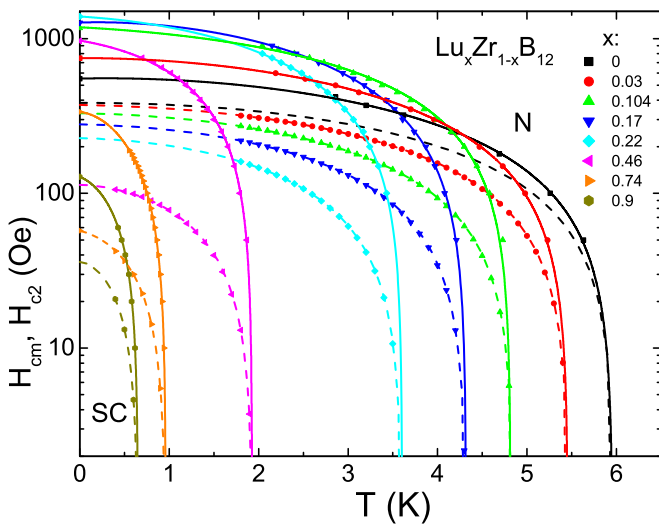


FIG. 9. Temperature dependencies of the thermodynamic  $H_{cm}(T)$  and upper  $H_{c2}(T)$  critical fields, resulting from the heat capacity analysis. SC and N denote the superconducting and normal states. Solid and dashed lines show the fits to highlight  $H_{cm}(0)$  and  $H_{c2}(0)$  values.

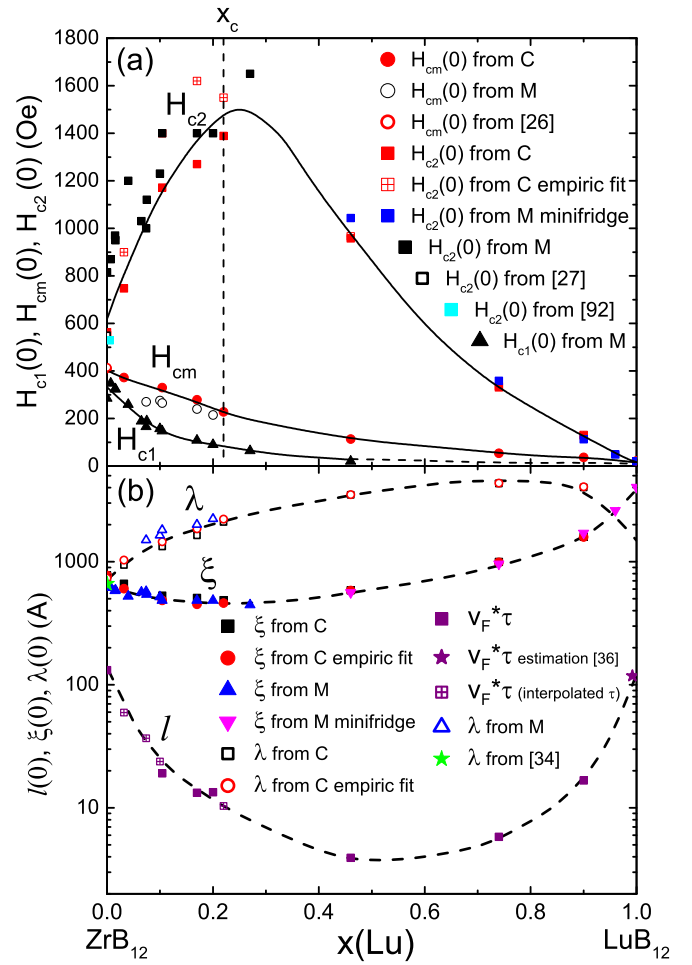


FIG. 10. Concentration dependencies of (a) the critical fields  $H_{c1}(0)$ ,  $H_{cm}(0)$ , and  $H_{c2}(0)$ , and (b) the coherence length  $\xi(0)$ , the penetration depth  $\lambda(0) = \kappa_{1,2}(0)\xi(0)$ , and the mean free path of charge carriers  $l(x)$ .

with derivatives  $dH_{c2}/dT$  at  $T = T_c$  obtained from the experimental data. Using the electronic specific heat coefficient  $\gamma(x)$  [Fig. 8(a)], the bare density of electronic states (DOS) at the Fermi level  $N_b(E_F) = 0.122(\text{eV atom})^{-1}$  for  $\text{ZrB}_{12}$  and  $N_b(E_F) = 0.108(\text{eV atom})^{-1}$  for  $\text{LuB}_{12}$  known from band structure calculations [35,40,53,63–66] and the relation

$$\gamma = 1/3\pi^2 k_B^2 N_b(E_F)(1 + \lambda_{e\text{-ph}}) \quad (8)$$

( $k_B$  is the Boltzmann constant), we have estimated the electron-phonon interaction constant  $\lambda_{e\text{-ph}}(x)$  [see inset in Fig. 8(b),  $N_b(E_F)$  values for various Lu content were taken by the linear interpolation between DOS of  $\text{LuB}_{12}$  and  $\text{ZrB}_{12}$ ] which for parent compounds  $\text{LuB}_{12}$  and  $\text{ZrB}_{12}$  is in good agreement with results of [26–28]. For independent evaluation of the renormalized  $N(E_F) = N_b(E_F)(1 + \lambda_{e\text{-ph}})$  and  $\lambda_{e\text{-ph}}$  we use also the relation

$$\Delta C/T_c = 0.95\pi^2 N(E_F), \quad (9)$$

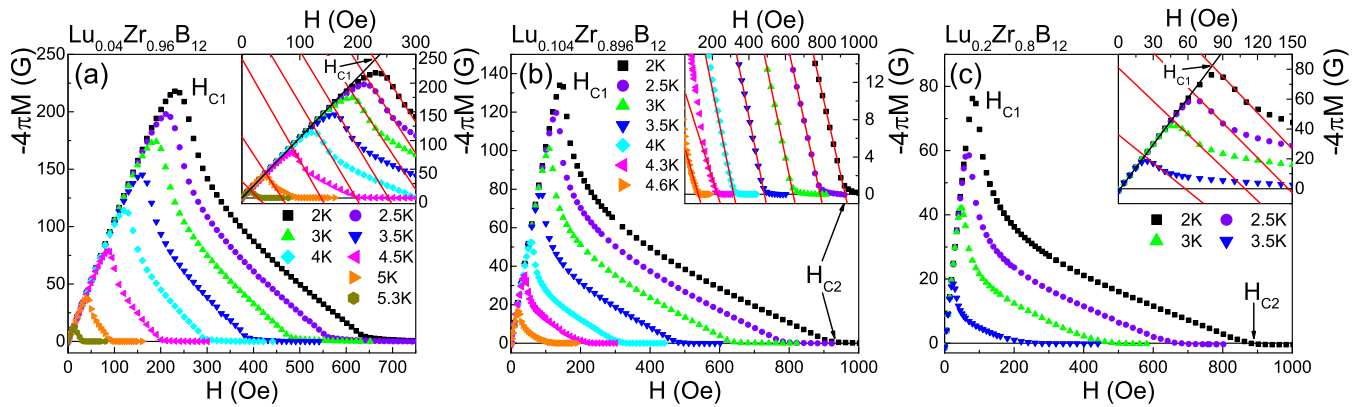


FIG. 11. The diamagnetic  $M(H, T_0)$  dependencies of  $\text{Lu}_x\text{Zr}_{1-x}\text{B}_{12}$  samples with  $x = 0.04, 0.1,$  and  $0.2$  [(a), (b), and (c), respectively]. The procedure usually applied for the extraction of critical fields  $H_{c1}$  and  $H_{c2}$  is shown in the insets.

which links the jump of heat capacity at  $T_c$  with  $N(E_F)$  in the family  $\text{Lu}_x\text{Zr}_{1-x}\text{B}_{12}$  superconductors [see  $\Delta C/T_c(x)$  dependence in Fig. 8(b)]. Then, from BCS relations

$$\Delta(0) = [2\pi N(E_F)]^{-1/2} H_{cm}(0), \quad (10)$$

$$\xi(0) = (\Phi_0/2\pi H_{c2})^{1/2}, \quad (11)$$

$$\kappa_1(T) = 2^{-1/2} H_{c2}(T)/H_{cm}(T), \quad (12)$$

where  $\Phi_0$  denotes the flux quantum, the GLM parameter  $\kappa_1(T)$  [67] (see Fig. S16 in [48]), the single-band average superconducting gap  $\Delta(0)$  [Fig. 6(b)], the coherence length  $\xi(0)$ , and the penetration depth  $\lambda(0) = \kappa_{1,2}(0)\xi(0)$  [Fig. 10(b)] could be calculated. For a few  $\text{Lu}_x\text{Zr}_{1-x}\text{B}_{12}$  magnetic crystals the evaluation of the Sommerfeld coefficient  $\gamma$  was obtained from the dimensionless ratio  $\gamma T_c^2/\mu_0 V H_{cm}^2(0) = \text{const}$  [26,68,69]. This last invariant was estimated to be  $1.95 \pm 0.15$  for  $\text{ZrB}_{12}$  and ranging in the interval 2–2.2 for other  $\text{Lu}_x\text{Zr}_{1-x}\text{B}_{12}$  compositions in accordance with  $s$ -wave pairing [68] and being only slightly above the BCS value 0.17 [70]. An average gap ratio of  $2\Delta/k_B T_c = 3.7 \pm 0.15$  was found for all  $\text{Lu}_x\text{Zr}_{1-x}\text{B}_{12}$  samples except  $\text{LuB}_{12}$  where  $2\Delta/k_B T_c = 3.2 \pm 0.1$  was calculated. Note that in the case of  $\text{ZrB}_{12}$  and  $\text{LuB}_{12}$  the gap to  $T_c$  ratio coincides very well with the results obtained from the heat capacity analysis of [26–28,36] and for  $\text{ZrB}_{12}$  it exceeds slightly the value of 3.52 of the BCS model. It is also worth noting that surface sensitive techniques provide much more higher ratios, 4.8 in Andreev reflection experiments [32], 4.15 [71] and  $4.75 \pm 0.1$  [30] in the point-contact and tunnel spectra measurements, correspondingly, and  $4.77 \pm 0.04$  in  $\text{ZrB}_{12}$  powder magnetization studies [72]. These differences have been pointed out by Tsindlekht *et al.* [30,31,73] and explained by enhanced surface characteristics of  $\text{ZrB}_{12}$  leading to rather different superconducting properties of bulk [26,27,30,33,65,74] and surface [30–32,34,71–73].

When discussing finally the superconducting characteristics in terms of  $s$ -wave weak coupling BCS superconductors [ $\lambda_{e\text{-ph}} \leq 0.4$ , see inset in Fig. 8(b)] note that even in case of  $\text{ZrB}_{12}$  the quality of the  $\alpha$ -model fit

$$C_s(T) = A_0 T^{-3/2} \exp[-\Delta(0)/k_B T], \quad (13)$$

is not adequate to describe the electronic specific heat, and the two-gap or anisotropic gap scenarios (see [24], for details) look like a better fitting approximation [see Figs. 5(b) and 5(c)]. Figure 6(b) shows the changes of the two-gap  $\alpha$ -model parameters  $\Delta_1(0)$  and  $\Delta_2(0)$  in the family  $\text{Lu}_x\text{Zr}_{1-x}\text{B}_{12}$  and the inset presents the  $x$  dependence of the relative weight  $n_2(x)$  of the small-gap component.

#### D. Magnetization

Below the transition temperature  $T_c$  a diamagnetic response is detected on magnetization curves  $M(T)$  [Fig. 2(d)] in very small magnetic fields (1–6 Oe). Note that a strong paramagnetic Meissner effect (PME) has been observed previously in studies of  $\text{ZrB}_{12}$  single crystals [75], and the PME was related to superconducting surface states [76]. However, within the limit of experimental accuracy we have not found any influence of PME on the magnetic characteristics of the superconducting state of studied  $\text{Lu}_x\text{Zr}_{1-x}\text{B}_{12}$  samples. An increase of external magnetic field up to 1 kOe leads to the appearance of features on  $M(H, T_0)$  curves which are typical for type-II superconductors. Indeed, a linear rise of the diamagnetic magnetization is observed in the range below the lower critical field  $H < H_{c1}$  corresponding to Meissner phase with about total ( $\sim 100\%$ , see also Fig. S15 in [48]) response, and above  $H_{c1}$ , in the mixed state,  $M(H)$  decreases dramatically until the transition to normal state at the upper critical field  $H_{c2}$  occurs. Figure 11 demonstrates the diamagnetic  $M(H, T_0)$  dependencies as obtained for  $\text{Lu}_x\text{Zr}_{1-x}\text{B}_{12}$  samples with  $x = 0.04, 0.1,$  and  $0.2$  [Figs. 11(a), 11(b) and 11(c), respectively]. The procedure usually applied for the extraction of critical fields is shown in the insets of Fig. 11, where the intersection points of linear asymptotics marked as  $H_{c1}$  and  $H_{c2}$  are shown for various temperatures. The values of  $H_{c1}$  were corrected to the demagnetization factor. The received behavior of the critical fields for Zr-rich crystals of  $\text{Lu}_x\text{Zr}_{1-x}\text{B}_{12}$  is presented in Fig. S17 in [48]. The normalized dependencies  $h_{c1} = H_{c1}/H_{c1}(0)$  vs  $(T/T_c)$  and  $h_{c2} = H_{c2}/H_{c2}(0)$  vs  $(T/T_c)$  scaled very well for all Zr-rich samples and these almost coincide with each other (Fig. S17 in [48]) and with commonly used phenomenological and BCS approximations.



The analysis of magnetization was carried out based on formulas which are well known from the Abrikosov theory of type-II superconductivity [77]

$$-4\pi M = (H_{c2} - H) / [(2\kappa_2^2 - 1)\beta_\Delta], \quad (14)$$

$$H_{c1}(T) = H_{c2} / [2\kappa_2^2 (\ln \kappa_2 + a)], \quad (15)$$

where  $\kappa_2$  is the GLM parameter [67,77,78],  $\beta_\Delta = 1.16$  is the coefficient corresponding to a triangular lattice of Abrikosov vortices, and  $a$  is the constant depending on impurity concentration. Presented in Fig. 11 are the linear dependencies of magnetization  $M(H)$  in the superconducting phase near  $H_{c2}$  which allow us to derive the  $\kappa_2(T)$  behavior within the framework of Eq. (14) (see Fig. S16 in [48]). Then the extrapolation to zero temperature provides values of  $\kappa_2(0)$  [Fig. 3(c)] and  $a$  (not shown) parameters. In addition, we use Eq. (11) to estimate the coherence length  $\xi(0)$  and the penetration depth  $l(0) = \kappa_2(0)\xi(0)$ ;  $H_{c1}(0)$  [see Fig. 10(b)] was defined from magnetization data of Fig. 11. The comparison of GLM parameters  $\kappa_1(T)$  and  $\kappa_2(T)$  [67,77,78] for  $\text{Lu}_x\text{Zr}_{1-x}\text{B}_{12}$  crystals with  $x = 0.104$  and  $0.17$  obtained from the analysis of heat capacity [Eq. (12)] and magnetization [Eq. (14)], respectively, shows that  $\kappa_1$  and  $\kappa_2$  differ noticeably (up to 20%, see Fig. S16 in [48]), arguing in favor of inhomogeneous superconductivity in these nonequilibrium compounds with dynamic charge stripes. According to the recommendations of [70] the heat capacity data were considered as superior to the results of magnetization measurements in determining  $H_{c2}(T)$ . Taking into account strong enhancement of superconductivity in the surface layer of  $\text{ZrB}_{12}$  [30–32,34,71–73], we have not studied here the resistivity changes in magnetic field near  $T_c$  in the  $\text{Lu}_x\text{Zr}_{1-x}\text{B}_{12}$  crystals.

## IV. DISCUSSION

### A. Order-disorder transition and pseudogap state

The formation of two-level systems in dodecaborides has been observed experimentally in  $\text{LuB}_{12}$  [47] and  $\text{ZrB}_{12}$  [33] where Lu/Zr ions are embedded in large size cavities arranged by  $\text{B}_{24}$  cubo-octahedra (see Fig. 1). In Raman spectra of  $\text{Lu}^N\text{B}_{12}$  [47] and  $\text{Zr}^N\text{B}_{12}$  [79] with a different isotopic composition of boron ( $N = 10, 11$ , nat; nat corresponds to the natural content of boron isotopes: 18.83%  $^{10}\text{B}$  and 81.17%  $^{11}\text{B}$ ) it was shown that the Raman response exhibits a boson peak at liquid nitrogen temperatures, and such a feature in the low-frequency range was discussed as a fingerprint of systems with strong structural disorder. To explain the properties of  $\text{LuB}_{12}$  authors of [47] have proposed a model of cage-glass formation with a phase transition at  $T^* \sim 50\text{--}70$  K, and it was found that the barrier height of the double-well potential  $\Delta E_2$  [Fig. 1(e)] is practically equal to the cage-glass transition temperature  $T^*$ . In  $\text{ZrB}_{12}$  the order-disorder transition was found at  $T^* \sim 90\text{--}100$  K [37] and  $\Delta E_2$  and  $T^*$  parameters are about equal to the pseudogap  $\Delta_{\text{ps-gap}} = 7.3 \pm 2$  meV detected by the high resolution photoemission spectroscopy of zirconium dodecaboride [35]. It was shown in [33,47] that the temperature lowering at  $T < T^*$  leads to displacements of metallic ions from their central positions inside the  $\text{B}_{24}$  cubo-octahedra (see Figs. 1(d) and 1(e) and also [55,56]). The

result is a static disorder in the arrangement of  $\text{Lu}^{3+}(\text{Zr}^{4+})$  ions while maintaining the rigid covalent boron framework (the so-called cage-glass state).

The presence of two-level systems with a barrier of  $\Delta E_2 \sim 90$  K was reliably demonstrated also in cage-glass compound  $\text{LaB}_6$  and in  $\text{Ce}_x\text{La}_{1-x}\text{B}_6$  solid solutions basing on low temperature heat capacity measurements [80,81]. Furthermore, a pseudogap [82] and a low-frequency peak in inelastic light scattering spectra [83,84] were found in  $\text{LaB}_6$  and the barrier in the DWP was attributed to the formation of a pseudogap in disordered metallic systems [80,81]. Later on similar conclusions were made for  $\text{YB}_6$  where the cage-glass transition at  $T^* \sim 50$  K was found to be accompanied by the appearance of a DWP barrier of  $\Delta E_2 \sim 50$  K and it was discussed in terms of pseudogap emergence [85]. It is worth noting that all these high borides are characterized by small enough residual resistivity values located in the range  $0.01\text{--}50$   $\mu\text{Ohm cm}$  and their conduction bandwidth is about  $1.6\text{--}2$  eV (see, e.g., [28,38,39,65,86]), so the pseudogap may be considered as a merit of disorder and anharmonicity in these good metals.

The  $\Delta_{\text{ps-gap}}(x) = \Delta E_2(x)$  changes in the  $\text{Lu}_x\text{Zr}_{1-x}\text{B}_{12}$  family are detected from the analysis of heat capacity (see, for example, Fig. S10 in [48]) elucidating the location of the pseudogap area just above the superconducting state on the phase diagram of these nonequilibrium metals (Fig. 6). A source of lattice instability in  $\text{LuB}_{12}$  and another RE and transition metal dodecaborides is related to the cooperative Jahn-Teller instability of  $\text{B}_{12}$  clusters (ferro-distortive effect), which manifests both the emergence of small static distortions of the fcc lattice and the formation of dynamic charge stripes along unique [110] direction depending on the distribution of impurities and imperfections [42–45,87,88]. According to the conclusions [43,44,87] the infinite cluster of stripes appears only in the disordered phase below  $T^*$ , but the fcc lattice instability develops in  $\text{RB}_{12}$  with temperature lowering well above  $T^*$  approaching the Ioffe-Regel limit near  $T_E \sim 150$  K, where the vibrational density of states reaches the maximum [47] and strong changes appear both in structural parameters and characteristics of the atomic dynamics [44,88–90]. It is worth noting finally in this section that the pseudogap  $\Delta_{\text{ps-gap}}(x)$  decreases only slightly in the range  $0 \leq x \leq 0.9$  in  $\text{Lu}_x\text{Zr}_{1-x}\text{B}_{12}$  where we observe an order of magnitude  $T_c$  changes, but for  $\text{LuB}_{12}$  crystals  $\Delta_{\text{ps-gap}}$  depresses essentially taking values of  $60\text{--}80$  K depending on the concentration of boron vacancies (see Fig. 6(a) and [47] for more details).

Thus, the pseudogap evolution is not directly related to  $T_c$ , being in contrast with the behavior observed in the HTSC cuprates, where, e.g., the pseudogap coexists with superconducting gap over the whole superconducting dome, and decreases and disappears above an optimal hole doping [5].

### B. Lengths and limits

When discussing the superconducting characteristics of the parent  $\text{ZrB}_{12}$  compound it should be pointed out that since zirconium dodecaboride has a GLM parameter  $\kappa$  very close to the threshold value  $\kappa_c = 1/\sqrt{2}$ , small changes in the sample preparation process (e.g., defect concentration and thermal treatment) result in a variation of  $\kappa$  between type-I and type-II superconductivity [see Fig. 3(b)]. In our  $\text{ZrB}_{12}$  samples

typical  $\kappa$  values were detected between 0.8 and 1.14 [74], but the purest crystals are type-I superconductors with  $\kappa \sim 0.65$  [26,27]. Note that the location of  $\text{ZrB}_{12}$  near  $\kappa_c$  allows detecting both type-I and type-II [26,27] and type-II and type-II/1 [75,91] crossovers with the temperature lowering (see inset in Fig. 3(b) and [26,27,91] for more details). Moreover, the growth of  $\text{ZrB}_{12}$  crystals is a very complicated process [48], so the coexistence of type-I and type-II superconducting areas are typical, and this kind of inhomogeneity of crystals was directly observed in the  $\mu\text{SR}$  studies of zirconium dodecaboride [92]. The correlation length and the penetration depth estimated in the present study for  $\text{ZrB}_{12}$  are in the range  $\xi(0) \sim \lambda(0) \sim 680\text{--}780 \text{ \AA}$  [Fig. 10(b)]. Our evaluation of the mean free path of charge carriers  $l(0)$  from residual resistivity  $\rho_0$  (Fig. 2), from the Hall coefficient  $R_H$  (Fig. 4 and [48]), and from parameters  $\xi(0)$  [Fig. 10(b)] and  $\Delta(0)$  [Fig. 6(b)] lead within the framework of standard relations

$$l = R_H m^* v_F / (e \rho_0), \quad (16)$$

$$\xi(0) = \hbar v_F / [\pi \Delta(0)] \quad (17)$$

( $v_F$  is the average Fermi velocity [see Fig. 8(b)] and  $m^*$  is the effective mass  $m^* \sim 0.7m_0$  [52]) to a value of  $l \sim 130 \text{ \AA}$  for the studied  $\text{ZrB}_{12}$  crystals [see Fig. 10(b)]. This results into a ratio  $\xi/l \sim 5$  validating the “dirty limit” superconductivity even for the “pure” parent compound. Note the obtained Fermi velocity  $v_F(\text{ZrB}_{12}) \sim 3.5 \times 10^7 \text{ cm/s}$  [Fig. 8(b)] differs strongly from the rough Drude-type estimation  $v_F(\text{ZrB}_{12}) \sim 1.9 \times 10^8 \text{ cm/s}$  [34]. Moreover, the average Fermi velocity decreases dramatically with the change of lutetium concentration in the range  $x(\text{Lu}) < 0.8$ , starting to increase slightly in Lu-rich solid solutions [Fig. 8(b)]. On the contrary, the charge transport relaxation time  $\tau(\text{ZrB}_{12}) = 3.7 \times 10^{-14} \text{ s}$  derived here [Fig. 4(e)] is in agreement with the results deduced from optical studies ( $\tau = 4.2 \times 10^{-14} \text{ s}$  [28,65]), high resolution photoemission spectroscopy ( $\tau = 6 \times 10^{-14} \text{ s}$  [35]), and de Haas–van Alphen quantum oscillations measurements ( $\tau = 1.7\text{--}7.4 \times 10^{-14} \text{ s}$  [52], see also estimation [106]). It is worth noting also that a huge value of the Fermi surface averaged Dingle temperature  $T_D = \hbar/2\pi k_B \tau \sim 70 \text{ K}$  [52] argues in favor of very strong charge carrier scattering in this inhomogeneous superconductor.

It is seen from Fig. 3(b) that in the range  $0 < x < 0.95$  the  $\text{Lu}_x\text{Zr}_{1-x}\text{B}_{12}$  solid solutions are type-II superconductors, and the GLM parameter reaches its maximum value  $\kappa \sim 6$  in crystals with  $x \sim 0.5$  corresponding to the highest substitutional disorder [Fig. 3(b)]. Note that the  $\kappa_{1,2}(x)$  dependence [Fig. 3(b)] correlates very well with the residual resistivity  $\rho_0(x)$  changes [Fig. 3(a)] and with the relaxation rate  $\tau^{-1}(x)$  [Fig. 4(e)], so the well-known relation

$$\kappa_d = \kappa_p + 7.53 \times 10^3 \rho_0 \gamma^{1/2} \quad (18)$$

(see, e.g., [93],  $\kappa_d$  and  $\kappa_p$  are GLM parameters in the dirty and pure limits, correspondingly) is at least valid qualitatively. Both in  $\text{LuB}_{12}$  and in Lu-rich crystals with  $x > 0.95$  the type-I superconductivity recovers. Indeed, it is certainly demonstrated in Fig. 12 that the BCS relation Eq. (6) describes very well the temperature dependence of the critical field only for Lu-rich samples, but the type-II behavior  $h_{c2}(t) = (1 - t^2)/(1 + t^2)$ , where  $h_{c2} = H_{c2}/H_{c2}(0)$

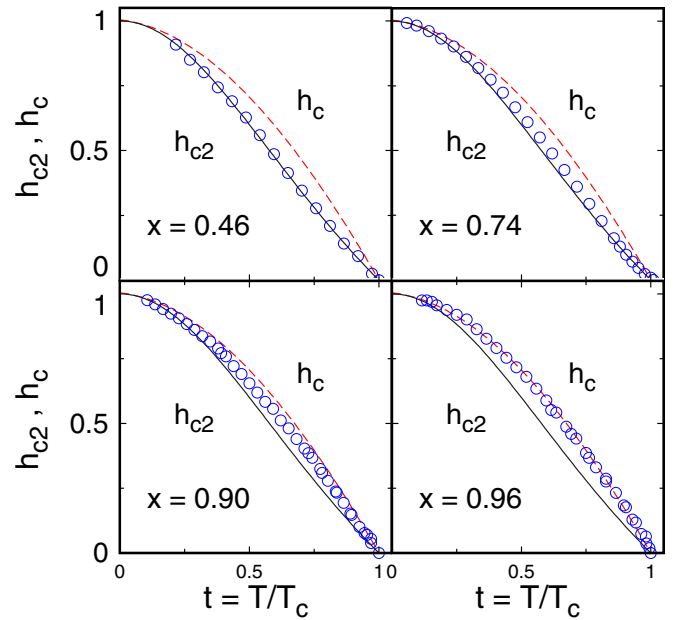


FIG. 12. Temperature dependencies of the normalized field of superconductivity suppression in Lu-rich  $\text{Lu}_x\text{Zr}_{1-x}\text{B}_{12}$  samples in comparison with the BCS formula Eq. (6) for the thermodynamic critical field and with the empiric relation  $h_{c2}(t) = (1 - t^2)/(1 + t^2)t = T/T_c$  for the upper critical field.

and  $t = T/T_c$  becomes valid in the concentration range  $x \leq 0.74$ . So, Lu-rich compounds are type-I superconductors characterized by very small  $T_c$  [Fig. 6(a)] and critical field  $H_{cm}$  [Fig. 10(b)], and with a large enough size of Cooper pairs  $\xi(\text{LuB}_{12}) \sim 4000 \text{ \AA}$  [Fig. 10(a)]. It is worth noting that  $\xi/l \sim 36$  is detected for  $\text{LuB}_{12}$  and this ratio increases strongly reaching the largest value  $\xi/l \sim 150$  near  $x \sim 0.5$  where  $l \sim r(\text{R-R}) \sim 5 \text{ \AA}$  [ $r(\text{R-R})$  is the distance between heavy Zr/Lu ions in the fcc lattice, see Fig. 1(a)] and validating the dirty limit superconductivity for all  $\text{Zr}_{1-x}\text{Lu}_x\text{B}_{12}$  compounds. Evidently these huge  $\xi/l$  ratios should be considered as a consequence of the JT lattice instability and of the dynamic charge stripes, resulting in very strong charge carrier scattering in inhomogeneous superconductors with nanoscale electron phase separation [see Figs. 1(a)–1(c)].

When the Lu content increases in the range  $x \leq x_c$  in  $\text{Lu}_x\text{Zr}_{1-x}\text{B}_{12}$  the  $T_c(x)$  [Fig. 6(a)] and correlation length  $\xi(x)$  [Fig. 10(b)] demonstrate a moderate decrease which is accompanied by a similar decrease of (i) the Sommerfeld coefficient  $\gamma(x)$ , (ii) the concentration of charge carriers  $n_e/n_R(x) = 1/(R_H e n_R)$  ( $n_R$  is the concentration of R ions in  $\text{RB}_{12}$ ), and (iii) the jump of heat capacity  $\Delta C/T_c(x)$  [Figs. 8(a) and 8(b)]. Taking into account that all these parameters  $\gamma(x)$ ,  $n_e/n_R(x)$ , and  $\Delta C/T_c(x)$  are the characteristics of the renormalized DOS  $N(E_F) = N_b(E_F)(1 + \lambda_{e\text{-ph}})$  it is natural to attribute the weakening of superconductivity to the moderate lowering of  $\lambda_{e\text{-ph}}(x)$  in the range  $x \leq x_c$  [see inset in Fig. 8(b)]. We need to note that the conservation of parameter  $2\Delta/k_B T_c = 3.7 \pm 0.15$ , which is close to BCS value 3.52, for all  $\text{Lu}_x\text{Zr}_{1-x}\text{B}_{12}$  with  $x \leq 0.95$ , from one side, and the good quality scaling detected for the critical fields  $h_{c1}(t)$  and  $h_{c2}(t)$  in the range  $x \leq x_c$  (see Fig. S17 in [48]), from another, argue in favor of

common BSC type description of dirty limit superconductivity in Zr-rich solid solutions.

### C. Scenarios of superconductivity

Properties of the superconducting state of conventional, single-band, electron-phonon superconductors are well described within isotropic Eliashberg theory with a single electron-phonon spectral density  $\alpha^2(\omega)F(\omega)$  for the average interaction over the Fermi surface [69,94]. Despite the Eliashberg function for various electrons, the Fermi surface is anisotropic leading to energy gap anisotropy, usually in the dirty limit superconductors where the electron mean free path is much smaller than the coherence length, only Fermi surface averaging of the electron-phonon spectral density can be used. This is not the case of  $\text{Lu}_x\text{Zr}_{1-x}\text{B}_{12}$  although the  $\xi/l$  ratio ranges in limits 5–150 (Fig. 10). Indeed, both BCS and strong coupling single-band scenarios with the deduced constant  $\lambda_{\text{e-ph}} \leq 0.4$  [see inset in Fig. 8(b)] and with the pre-exponent  $\langle \hbar\omega_{\text{in}} \rangle / k_{\text{B}} \approx \theta_{\text{E}} = 160\text{--}200\text{ K}$  corresponding to Cooper pairing mediated by quasilocal vibrations (rattling modes) of Zr/Lu ions cannot explain both the  $T_{\text{c}}(\text{ZrB}_{12}) \approx 6\text{ K}$  and the  $T_{\text{c}}$  changes in solid solutions. For instance, within the framework of the Allen-Dynes relation for superconducting transition temperature [95]

$$k_{\text{B}}T_{\text{c}} = \frac{\hbar\omega_{\text{in}}}{1.2} \exp \left[ -\frac{1.04(1 + \lambda_{\text{e-ph}})}{\lambda_{\text{e-ph}} - \mu^*(1 + 0.62\lambda_{\text{e-ph}})} \right] \quad (19)$$

in the case of  $\text{ZrB}_{12}$  we obtain curious, small, and negative Coulomb pseudopotential  $\mu^* \sim -0.02$ . On the contrary, when taking the traditional value  $\mu^* \sim 0.1$  we obtain  $\lambda_{\text{e-ph}}(\text{ZrB}_{12}) \approx 0.65$ , which is similar to the coupling constant calculated in [32], but is not in accord with the experimental heat capacity results (see inset in Fig. 8(b) and [26–28]). Similar estimation  $\lambda_{\text{e-ph}} \approx 0.68$  was found from the analysis of the low temperature optical reflectivity spectra of  $\text{ZrB}_{12}$  using the isotropic transport Eliashberg function  $\alpha^2(\omega)F(\omega)$  which has two peaks around 12 and 60 meV [65]. According to [28,36,65,79] a low frequency peak in the Eliashberg function was observed in  $\text{ZrB}_{12}$  near  $\omega_0 \sim 100\text{ cm}^{-1}$  ( $\sim 12\text{ meV}$ ) and it is located well below the Einstein mode at  $\omega_{\text{E}} \sim 140\text{ cm}^{-1}$  ( $\sim 17.5\text{ meV}$ ) [29]. The value  $\lambda_{\text{e-ph}} \approx 0.58$  was deduced from the detailed analysis of heat capacity made in [33] where three Einstein modes  $\hbar\omega_{\text{E}1}/k_{\text{B}} \approx 200\text{ K}$  and  $\hbar\omega_{\text{E}2,3}/k_{\text{B}} \approx 450\text{ K}$  were found to mediate the electron-phonon interaction in  $\text{ZrB}_{12}$  resulting in pre-exponent  $\langle \hbar\omega_{\text{in}} \rangle / k_{\text{B}} \approx 368\text{ K}$ . Note again that the isotropic single-band models do not discuss the difference between the estimated values  $\lambda_{\text{e-ph}} \approx 0.58\text{--}0.68$  and the much smaller constant  $\lambda_{\text{e-ph}} \sim 0.4$  detected from the Sommerfeld coefficient (Fig. 8 and [26–28]).

The situation becomes much more appealing in the two-band scenario which is supported obviously by the two-gap  $\alpha$ -model fit of the heat capacity in the superconducting state of  $\text{Lu}_x\text{Zr}_{1-x}\text{B}_{12}$  [see, for example, Figs. 5(b) and 5(c)]. In this case we found  $\Delta_1(0) \sim 14\text{ K}$  and  $\Delta_2(0) \sim 6\text{ K}$  in Zr-rich crystals with  $x < x_{\text{c}}$  detecting a larger gap and a strong coupling limit ratio  $2\Delta_1/k_{\text{B}}T_{\text{c}} \approx 4.8$ . Similar gap values  $\Delta_1(0) \sim 14\text{ K}$  and  $\Delta_2(0) \sim 8\text{ K}$  were deduced in the rf measurements of  $\text{ZrB}_{12}$  [96]. The ratio for the smaller gap was estimated to be only  $2\Delta_2/k_{\text{B}}T_{\text{c}} \sim 2$ , and we suppose an essential interband

coupling and impurity scattering in these compounds with structural (cooperative JT effect of  $\text{B}_{12}$  clusters [43–45,87]) and electron [dynamic charge stripes, Figs. 1(a)–1(c)] instabilities. The strong difference between the larger and smaller gap ratio is similar to that one observed previously in archetypal two-band superconductor  $\text{MgB}_2$ , in  $\text{Lu}_2\text{Fe}_3\text{Si}_5$ , etc. (see, for example, [24] for review). Moreover, the larger gap  $\Delta_1(0) \sim 14\text{ K}$  is about equal to values  $\sim 14\text{--}15\text{ K}$  observed for  $\text{ZrB}_{12}$  in surface sensitive experiments [30,32,71,72]. The unique enhanced surface superconductivity in  $\text{ZrB}_{12}$  [31,73] was explained in [97] in the framework of the self-organized percolative theory of superconductivity [98] suggesting the formation of a filamentary network and disorder-enhanced electron-phonon coupling at the surface. The authors [72] considered the possibility of nonadiabatic coupling of charge carriers to the crystal lattice appearing in  $\text{ZrB}_{12}$  close to the surface. The difference between the surface and bulk state in  $\text{ZrB}_{12}$  has been studied in [99] using high resolution x-ray spectroscopy which reveals boron deficiency at the surface while the bulk is stoichiometric. Correspondingly, in the two-band scenario of superconductivity in  $\text{ZrB}_{12}$  one needs to suppose that the enhanced surface characteristics may be related to the suppression of the smaller superconducting gap in the surface layer.

It is interesting to note that similar values  $2\Delta_1/k_{\text{B}}T_{\text{c}} \approx 4.8$  and  $2\Delta_2/k_{\text{B}}T_{\text{c}} \sim 2$  were predicted for the gap ratios in two-band *s*-wave superconductors in detailed Eliashberg calculations developed in [94]. For the coupling constants  $\lambda_{11} = 1$  and  $\lambda_{22} = 0.1$  in the upper and lower bands authors [94] obtained  $\lambda_{12} \approx 0.4$  and  $\lambda_{21} \approx 0.3$  for the off-diagonal interband elements of the electron-phonon interaction (see Fig. 3 in [94]) confirming the case of an essential interband coupling in  $\text{Lu}_x\text{Zr}_{1-x}\text{B}_{12}$ . A comparison of the calculated and experimental cyclotron mass made in studies of the de Haas–van Alphen effect showed unusually large electron-phonon interaction on the neck ( $\lambda_{\text{e-ph}} \approx 0.95$ ) and box ( $\lambda_{\text{e-ph}} \approx 1.07$ ) sections of the Fermi surface of  $\text{ZrB}_{12}$  [52]. Similar estimation  $\lambda_{\text{e-ph}} \approx 1.0 \pm 0.3$  was obtained in optical measurements [65] indicating a strong coupling in  $\text{ZrB}_{12}$ . Note also that in the two-band scenario the volume averaged quasiparticle density of states at the Fermi surface is expected to be not large, providing small enough values of the Sommerfeld coefficient, but the DOS in the upper band at temperatures above  $T_{\text{c}}$  should be much higher. So the contradiction between small experimental  $\gamma$  and the deduced  $\lambda_{\text{e-ph}} \sim 0.4$  values, from one side, and large DOS and upper band coupling  $\lambda_{\text{e-ph}} \approx 1.0$ , from the other seems to be removed. Taking into account that the zeroing of heat capacity in the superconducting state is observed up to threshold-temperature  $\sim 0.2T_{\text{c}}$  [Figs. 5(b) and 5(c)], we conclude also in favor of the *s*-wave superconductivity, while in *d*-wave systems the gap nodes allow a significant occupation of the excitation spectrum at any finite temperature, which makes  $C/\gamma T$  to increase strongly even at very low temperatures [24]. Another argument in favor of *s*-wave superconductivity in  $\text{Lu}_x\text{Zr}_{1-x}\text{B}_{12}$  is the small enough dimensionless ratio  $\gamma T_{\text{c}}^2 / \mu_0 V H_{\text{cm}}^2(0) = 1.95\text{--}2.2$  which is nearly twice smaller as that predicted for the *d*-wave scenario in [68].

The two-band scenario of superconductivity in  $\text{Lu}_x\text{Zr}_{1-x}\text{B}_{12}$  has been proposed on the basis of  $\mu\text{SR}$  experiments to extract the superfluid density [41]. The

best fits to the  $\mu$ SR data on samples with low values of  $x$  were obtained with two-band models, with an  $s+d$  model giving the best fit [41]. However, there are many possible types of multigap behavior that may be realized outside the context of these simple models, and in particular the inclusion of impurity scattering and interband coupling can affect the detailed temperature dependence of the superfluid stiffness [24,94,100]. Therefore the  $\mu$ SR data [41], though strongly pointing to two-band superconductivity, could very well be consistent with two-band  $s$ -wave superconductivity in the presence of strong impurity scattering and interband coupling.

It is worth noting that in two-gap superconductors the specific effect of anisotropy may be attributed not only to the anisotropic electron-phonon interaction spectral function, but also could be described in terms of the anisotropy of Fermi velocity [101]. For instance, the upper critical field  $H_{c2}(T)$  depends on the orientation of applied magnetic field  $\mathbf{H}$  due to the anisotropy of Fermi velocity and its positive curvature near  $T_c$  may be considered as a measure of  $v_F$  anisotropy [24]. Figure 12 shows that the positive curvature emerges and grows with decreasing of Lu content in  $\text{Lu}_x\text{Zr}_{1-x}\text{B}_{12}$  solid solutions. The positive curvature of  $H_{c2}(T)$  near  $T_c$  is conserved in the range  $x < 0.5$  (see Fig. S17 in [48]) giving evidence in favor of anisotropic Fermi velocity. In our opinion, a huge (about 5 times) decrease of average Fermi velocity  $v_F(x)$  [Fig. 8(b)] also argues in favor of strong interband coupling, impurity scattering, and very strong anisotropy of superconductivity in Zr-rich  $\text{Lu}_x\text{Zr}_{1-x}\text{B}_{12}$ . Note that the upper critical field  $H_{c2}$  was one of the first properties of  $\text{MgB}_2$ , for which unconventional behavior was discerned, namely by a pronounced positive curvature of its temperature dependence near  $T_c$  [102–104]. Since then, this effect has been discovered in many compounds and considered as a confirmation of two-band superconductivity.

Following to [24] it should be pointed out, however, that the same effect on  $H_{c2}(T)$  occurs in *anisotropic single-band superconductors*. Moreover, different energy gap values, from which the smaller ones dominate the low- and the larger ones the high temperature behavior, are also found in anisotropic single-band superconductors. Accordingly, the resulting curves could easily resemble the two-band behavior [24]. Though it seems difficult to imitate the extreme two-band case, in which the contributions of the two gaps can still be distinguished (i.e., when interband effects are very weak). Most experimentally observed curves showing almost a linear or slightly convex behavior over large parts of the temperature range fit the anisotropic single-band model well, as was, e.g., demonstrated for  $\text{MgB}_2$  [105] (see also [24] for review). So the anisotropic single-band scenario cannot be ruled out for  $\text{Lu}_x\text{Zr}_{1-x}\text{B}_{12}$  and it should be verified in future in detailed magnetic field measurements of the heat capacity, superfluid density, etc.

Concluding the section we need to discuss the physical meaning of the critical behavior near  $x_c \sim 0.23$  where anomalies of residual resistivity  $\rho_0(x)$  and  $\alpha(x)$  (Fig. 3), of the Hall mobility  $\mu_H(x)$  and relaxation time  $\tau(x)$  (Fig. 4),  $T_c(x)$ , energy gaps  $\Delta_{1,2}(x)$ , and the relative weights of superconducting components  $n_i(x)$  (Fig. 6), of upper critical field  $H_{c2}(x)$  and correlation length  $\xi(x)$  (Fig. 10) are observed. Taking into account that fast fluctuations of electron density

(dynamic charge stripes detected near the rare earth (RE) ions in the fcc lattice of both  $\text{LuB}_{12}$  [42–44,87] and another RE dodecaborides [45,46]) and that an infinite cluster appears in the disordered cage-glass phase below  $T^* \sim 60$  K it seems natural to associate the anisotropy of superconductivity with these inhomogeneities and nanoscale phase separation in the matrix of  $\text{RB}_{12}$ . Moreover, in the filamentary structure the electron density fluctuations with frequency  $\sim 240$  GHz ( $\sim 1$  meV) [45] are arranged in the  $\text{RB}_{12}$  with trivalent rare earth ions in chains emerging near the RE ions which form channels along  $\langle 110 \rangle$  directions [43–46] and the Cooper pair breaking effect of these dynamic stripes becomes decisive. Evidently different configurations of fluctuating charges (checkerboard-type patterns instead of stripes) could be expected in the case of the transition metal dodecaboride with  $\text{Zr}^{4+}$  ions, where the wider conduction band is populated by two electrons per unit cell. At low temperatures  $T < T^*$  the infinite cluster develops and enforces above the percolation threshold ( $x \geq x_c \sim 0.23$ ), enhancing the pair breaking and depressing the superconductivity. Thus, even in the case of single-band superconductivity the anisotropy which is not removed in the dirty limit system with  $\xi/l = 5\text{--}150$  may be also explained by the cooperative JT instability of the boron sublattice which is accompanied with formation of a filamentary structure of fluctuating electron density in these inhomogeneous  $\text{Lu}_x\text{Zr}_{1-x}\text{B}_{12}$  solid solutions. The studies of fine details of crystal and electron structure in  $\text{ZrB}_{12}$  are in progress now and they promise to shed light on the features of Cooper pairing and pair breaking effects in these Zr-based superconductors.

## V. CONCLUSIONS

Normal and superconducting state characteristics have been studied in model strongly correlated electronic systems  $\text{Lu}_x\text{Zr}_{1-x}\text{B}_{12}$  with cooperative Jahn-Teller instability of boron sublattice and with nanoscale electron phase separation in form of dynamic charge stripes. It was shown that the purest  $\text{ZrB}_{12}$  and  $\text{LuB}_{12}$  crystals are type-I superconductors, and that Zr to Lu substitution induces immediately the type-I to type-II transition, whereas GLM parameters  $\kappa_{1,2}$  change in the range  $\kappa_{1,2} \leq 6$ . It was found that  $\text{Lu}_x\text{Zr}_{1-x}\text{B}_{12}$  are dirty limit superconductors with short enough mean free path  $l = 5\text{--}140$  Å and a coherence length changing nonmonotonously in the range 450–4000 Å (the ratio  $\xi/l = 5\text{--}150$ ). The most likely scenario proposed for these solid solutions is *two-gap s-wave superconductivity* with a strong coupling upper band ( $\lambda_{e\text{-ph}} \sim 1.0$ ,  $\Delta_1 \sim 14$  K, and  $2\Delta_1/k_B T_c \approx 4.8$ ) and weak coupling lower band ( $\lambda_{e\text{-ph}} \sim 0.1\text{--}0.4$ ,  $\Delta_2 \sim 6\text{--}8$  K, and  $2\Delta_2/k_B T_c \sim 2$ ), and with strong impurity scattering and interband coupling. At the same time we cannot exclude *anisotropic single-band superconductivity* with a strong anisotropic pair-breaking effect produced by dynamic charge stripes along  $\langle 110 \rangle$  directions. Moreover, a pseudogap state is detected in  $\text{Lu}_x\text{Zr}_{1-x}\text{B}_{12}$  with the  $\Delta_{\text{ps-gap}}$  values varying in the range 60–110 K. Also discussed is the mechanism responsible for the unique enhanced surface superconductivity in  $\text{ZrB}_{12}$ .

## ACKNOWLEDGMENTS

This work was supported in part by the Russian Science Foundation, Projects No. 17-12-01426 and No. 21-12-00186 and was performed using the equipment of the Shared Facility Center for Studies of HTSC and Other Strongly Correlated Materials, Lebedev Physical Institute, the Russian Academy

of Sciences, and of the Center of Excellence, Slovak Academy of Sciences. The work of K.F. and S.G. is supported by the Slovak agencies VEGA (Grant No. 2/0032/20) and APVV (Grant No. 17-0020). The authors are grateful to V. N. Krasnorussky for experimental assistance and B.P. Gorshunov for helpful discussions.

- [1] J. G. Bednorz and K. A. Müller, *Z. Phys. B: Condens. Matter* **64**, 189 (1986).
- [2] B. Keimer, S. A. Kivelson, M. R. Norman, S. Uchida, and J. Zaanen, *Nature (London)* **518**, 179 (2015).
- [3] E. Berg, E. Fradkin, S. A. Kivelson, and J. M. Tranquada, *New J. Phys.* **11**, 115004 (2009).
- [4] S. Sachdev and B. Keimer, *Phys. Today* **64**(2), 29 (2011).
- [5] S. Hüfner, M. A. Hossain, A. Damascelli, and G. A. Sawatzky, *Rep. Prog. Phys.* **71**, 062501 (2008).
- [6] E. Fradkin, S. A. Kivelson, M. J. Lawler, J. P. Eisenstein, and A. P. Mackenzie, *Annu. Rev. Condens. Matter Phys.* **1**, 153 (2010).
- [7] D. Reznik, *Phys. C Supercond.* **481**, 75 (2012).
- [8] Y. Kamihara, T. Watanabe, M. Hirano, and H. Hosono, *J. Am. Chem. Soc.* **130**, 3296 (2008).
- [9] X. H. Chen, T. Wu, G. Wu, R. H. Liu, H. Chen, and D. F. Fang, *Nature (London)* **453**, 761 (2008).
- [10] G. F. Chen, Z. Li, D. Wu, G. Li, W. Z. Hu, J. Dong, P. Zheng, J. L. Luo, and N. L. Wang, *Phys. Rev. Lett.* **100**, 247002 (2008).
- [11] M. Rotter, M. Tegel, and D. Johrendt, *Phys. Rev. Lett.* **101**, 107006 (2008).
- [12] R. M. Fernandes, A. V. Chubukov, and J. Schmalian, *Nat. Phys.* **10**, 97 (2014).
- [13] J. J. Lee, F. T. Schmitt, R. G. Moore, S. Johnston, Y.-T. Cui, W. Li, M. Yi, Z. K. Liu, M. Hashimoto, Y. Zhang *et al.*, *Nature (London)* **515**, 245 (2014).
- [14] P. J. Hirschfeld, M. M. Korshunov, and I. I. Mazin, *Rep. Prog. Phys.* **74**, 124508 (2011).
- [15] J. He, X. Liu, W. Zhang, L. Zhao, D. Liu, S. He, D. Mou, F. Li, C. Tang, Z. Li *et al.*, *Proc. Natl. Acad. Sci. USA* **111**, 18501 (2014).
- [16] G. R. Stewart, *Rev. Mod. Phys.* **83**, 1589 (2011).
- [17] R. Peng, X. P. Shen, X. Xie, H. C. Xu, S. Y. Tan, M. Xia, T. Zhang, H. Y. Cao, X. G. Gong, J. P. Hu *et al.*, *Phys. Rev. Lett.* **112**, 107001 (2014).
- [18] J. Nagamatsu, N. Nakagawa, T. Muranaka, Y. Zenitani, and J. Akimitsu, *Nature (London)* **410**, 63 (2001).
- [19] H. J. Choi, D. Roundy, H. Sun, M. L. Cohen, and S. G. Louie, *Phys. Rev. B* **66**, 020513 (2002).
- [20] J. Kortus, I. I. Mazin, K. D. Belashchenko, V. P. Antropov, and L. L. Boyer, *Phys. Rev. Lett.* **86**, 4656 (2001).
- [21] D. G. Hinks, H. Claus, and J. D. Jorgensen, *Nature (London)* **411**, 457 (2001).
- [22] S. L. Bud'Ko, G. Lapertot, C. Petrovic, C. E. Cunningham, N. Anderson, and P. C. Canfield, *Phys. Rev. Lett.* **86**, 1877 (2001).
- [23] X. X. Xi, *Rep. Prog. Phys.* **71**, 116501 (2008).
- [24] M. Zehetmayer, *Supercond. Sci. Technol.* **26**, 043001 (2013).
- [25] E. Dagotto, *Science* **309**, 257 (2005).
- [26] R. Lortz, Y. Wang, S. Abe, C. Meingast, Y. B. Paderno, V. Filippov, and A. Junod, *Phys. Rev. B* **72**, 024547 (2005).
- [27] Y. Wang, R. Lortz, Y. Paderno, V. Filippov, S. Abe, U. Tutsch, and A. Junod, *Phys. Rev. B* **72**, 024548 (2005).
- [28] J. Teyssier, R. Lortz, A. Petrovic, D. Van Der Marel, V. Filippov, and N. Shitsevalova, *Phys. Rev. B* **78**, 134504 (2008).
- [29] A. V. Rybina, K. S. Nemkovski, P. A. Alekseev, J.-M. Mignot, E. S. Clementyev, M. Johnson, L. Capogna, A. V. Dukhnenko, A. B. Lyashenko, and V. B. Filippov, *Phys. Rev. B* **82**, 024302 (2010).
- [30] M. I. Tsindlekht, G. I. Leviev, I. Asulin, A. Sharoni, O. Millo, I. Felner, Y. B. Paderno, V. B. Filippov, and M. A. Belogolovskii, *Phys. Rev. B* **69**, 212508 (2004).
- [31] G. I. Leviev, V. M. Genkin, M. I. Tsindlekht, I. Felner, Y. B. Paderno, and V. B. Filippov, *Phys. Rev. B* **71**, 064506 (2005).
- [32] D. Daghero, R. S. Gonnelli, G. A. Ummarino, A. Calzolari, V. Dellarocca, V. A. Stepanov, V. B. Filippov, and Y. B. Paderno, *Supercond. Sci. Technol.* **17**, S250 (2004).
- [33] N. Sluchanko, S. Gavrilkin, K. Mitsen, A. Kuznetsov, I. Sannikov, V. Glushkov, S. Demishev, A. Azarevich, A. Bogach, A. Lyashenko *et al.*, *J. Supercond. Nov. Magn.* **26**, 1663 (2013).
- [34] V. A. Gasparov, N. S. Sidorov, and I. I. Zver'Kova, *Phys. Rev. B* **73**, 094510 (2006).
- [35] S. Thakur, D. Biswas, N. Sahadev, P. K. Biswas, G. Balakrishnan, and K. Maiti, *Sci. Rep.* **3**, 3342 (2013).
- [36] K. Flachbart, S. Gabani, K. Gloos, M. Meissner, M. Opel, Y. Paderno, V. Pavlik, P. Samuely, E. Schuberth, N. Shitsevalova *et al.*, *J. Low Temp. Phys.* **140**, 339 (2005).
- [37] N. E. Sluchanko, A. N. Azarevich, M. A. Anisimov, A. V. Bogach, S. Y. Gavrilkin, M. I. Gilmanov, V. V. Glushkov, S. V. Demishev, A. L. Khoroshilov, A. V. Dukhnenko, K. V. Mitsen, N. Y. Shitsevalova, V. B. Filippov, V. V. Voronov, and K. Flachbart, *Phys. Rev. B* **93**, 085130 (2016).
- [38] H. Okamura, S. Kimura, H. Shinozaki, T. Nanba, F. Iga, N. Shimizu, and T. Takabatake, *Phys. Rev. B* **58**, R7496 (1998).
- [39] B. P. Gorshunov, E. S. Zhukova, G. A. Komandin, V. I. Torgashev, A. V. Muratov, Y. A. Aleshchenko, S. V. Demishev, N. Y. Shitsevalova, V. B. Filipov, and N. E. Sluchanko, *JETP Lett.* **107**, 100 (2018).
- [40] B. Jäger, S. Paluch, O. J. Zogał, W. Wolf, P. Herzig, V. B. Filippov, N. Shitsevalova, and Y. Paderno, *J. Phys.: Condens. Matter* **18**, 2525 (2006).
- [41] F. K. K. Kirschner, N. E. Sluchanko, V. B. Filipov, F. L. Pratt, C. Baines, N. Y. Shitsevalova, and S. J. Blundell, *Phys. Rev. B* **98**, 094505 (2018).
- [42] N. Sluchanko, A. Bogach, N. Bolotina, V. Glushkov, S. Demishev, A. Dudka, V. Krasnorussky, O. Khrykina, K. Krasikov, V. Mironov, V. B. Filipov, and N. Shitsevalova, *Phys. Rev. B* **97**, 035150 (2018).

- [43] N. B. Bolotina, A. P. Dudka, O. N. Khrykina, V. N. Krasnorussky, N. Y. Shitsevalova, V. B. Filipov, and N. E. Sluchanko, *J. Phys.: Condens. Matter* **30**, 265402 (2018).
- [44] N. B. Bolotina, A. P. Dudka, O. N. Khrykina, V. V. Glushkov, A. N. Azarevich, V. N. Krasnorussky, S. Gabani, N. Y. Shitsevalova, A. V. Dukhnenko, V. B. Filipov, and N. E. Sluchanko, *J. Phys. Chem. Solids* **129** 434 (2019).
- [45] N. E. Sluchanko, A. N. Azarevich, A. V. Bogach, N. B. Bolotina, V. V. Glushkov, S. V. Demishev, A. P. Dudka, O. N. Khrykina, V. B. Filipov, N. Y. Shitsevalova *et al.*, *J. Phys.: Condens. Matter* **31**, 65604 (2018).
- [46] A. L. Khoroshilov, V. N. Krasnorussky, K. M. Krasikov, A. V. Bogach, V. V. Glushkov, S. V. Demishev, N. A. Samarin, V. V. Voronov, N. Y. Shitsevalova, V. B. Filipov, S. Gabáni, K. Flachbart, K. Siemensmeyer, S. Y. Gavrilkin, and N. E. Sluchanko, *Phys. Rev. B* **99**, 174430 (2019).
- [47] N. E. Sluchanko, A. N. Azarevich, A. V. Bogach, I. I. Vlasov, V. V. Glushkov, S. V. Demishev, A. A. Maksimov, I. I. Tartakovskii, E. V. Filatov, K. Flachbart, S. Gabani, V. B. Filippov, N. Y. Shitsevalova, and V. V. Moshchalkov, *J. Exp. Theor. Phys.* **113**, 468 (2011); N. E. Sluchanko, A. N. Azarevich, S. Y. Gavrilkin, V. V. Glushkov, S. V. Demishev, N. Y. Shitsevalova, and V. B. Filippov, *JETP Lett.* **98**, 648 (2013).
- [48] See Supplemental Material at <http://link.aps.org/supplemental/10.1103/PhysRevB.103.104515> for details of the crystal growth of  $\text{Lu}_x\text{Zr}_{1-x}\text{B}_{12}$  substitutional solid solutions and samples characterization (Figs. S1–S7), field and temperature dependencies of magnetoresistance and Hall coefficient (Figs. S8 and S9), the heat capacity vs temperature (Fig. S10), heat capacity components in the normal and superconducting states and the data analysis (Figs. S11–S14), magnetization curves in the superconducting state (Fig. S15), temperature dependencies of GLM parameters (Fig. S16), and the scaling of thermodynamic and upper critical fields (Fig. S17).
- [49] J. Bačkai, S. Gabáni, K. Flachbart, E. Gažo, J. Kušnír, and M. Orendáč, *Acta Phys. Pol. A* **137**, 791 (2020).
- [50] N. E. Sluchanko, A. V. Bogach, V. V. Glushkov, S. V. Demishev, M. I. Ignatov, N. A. Samarin, G. S. Burkhanov, and O. D. Chistyakov, *J. Exp. Theor. Phys.* **98**, 793 (2004).
- [51] V. Gasparov, I. Sheikin, F. Levy, J. Teyssier, and G. Santi, *J. Phys.: Conf. Ser.* **150**, 052059 (2009).
- [52] V. A. Gasparov, I. Sheikin, F. Levy, J. Teyssier, and G. Santi, *Phys. Rev. Lett.* **101**, 097006 (2008).
- [53] M. Heinecke, K. Winzer, J. Noffke, H. Kranefeld, H. Grieb, K. Flachbart, and Y. B. Paderno, *Z. Phys. B: Condens. Matter* **98**, 231 (1995).
- [54] A. Czopnik, N. Shitsevalova, V. Pluzhnikov, A. Krivchikov, Y. Paderno, and Y. Onuki, *J. Phys.: Condens. Matter* **17**, 5971 (2005).
- [55] A. P. Menushenkov, A. A. Yaroslavtsev, I. A. Zaluzhnyy, A. V. Kuznetsov, R. V. Chernikov, N. Y. Shitsevalova, and V. B. Filippov, *JETP Lett.* **98**, 165 (2013).
- [56] H. Werheit, Y. Paderno, V. Filippov, V. Paderno, A. Pietraszko, M. Armbrüster, and U. Schwarz, *J. Solid State Chem.* **179**, 2761 (2006).
- [57] N. Sluchanko, A. Azarevich, A. Bogach, S. Gavrilkin, V. Glushkov, S. Demishev, K. Mitsen, N. Shitsevalova, V. Filippov, S. Gabani *et al.*, *Acta Phys. Pol. A* **131**, 1036 (2017).
- [58] C.-S. Lue, J. H. Ross Jr, C. F. Chang, and H. D. Yang, *Phys. Rev. B* **60**, R13941 (1999).
- [59] B. R. Coles, *Phys. B: Condens. Matter* **223**, 260 (1996).
- [60] K. A. Gschneidner Jr, J. Tang, S. K. Dhar, and A. Goldman, *Phys. B: Condens. Matter* **163**, 507 (1990).
- [61] J. R. Clem, *Ann. Phys. (NY)* **40**, 268 (1966).
- [62] N. R. Werthamer, E. Helfand, and P. C. Hohenberg, *Phys. Rev.* **147**, 295 (1966).
- [63] G. E. Grechnev, A. E. Baranovskiy, V. D. Fil, T. V. Ignatova, I. G. Kolobov, A. V. Logosha, N. Y. Shitsevalova, V. B. Filippov, and O. Eriksson, *Low Temp. Phys.* **34**, 921 (2008).
- [64] I. R. Shein and A. L. Ivanovskii, *Phys. Solid State* **45**, 1429 (2003).
- [65] J. Teyssier, A. B. Kuzmenko, D. Van Der Marel, F. Marsiglio, A. B. Liashchenko, N. Shitsevalova, and V. Filippov, *Phys. Rev. B* **75**, 134503 (2007).
- [66] X.-H. Li, Y.-L. Yong, H.-L. Cui, and R.-Z. Zhang, *J. Phys. Chem. Solids* **117** 173 (2018).
- [67] K. Maki, *Phys. Rev.* **148**, 362 (1966).
- [68] H. Chi and J. P. Carbotte, *Phys. Rev. B* **49**, 6143 (1994).
- [69] J. P. Carbotte, *Rev. Mod. Phys.* **62**, 1027 (1990).
- [70] T. G. Berlincourt, *Rev. Mod. Phys.* **36**, 19 (1964).
- [71] J. Girovsk'y, P. Szabo, T. Mori, and P. Samuely, *Acta Phys. Pol. A* **118**, 1042 (2010).
- [72] R. Khasanov, D. Di Castro, M. Belogolovskii, Y. Paderno, V. Filippov, R. Brüttsch, and H. Keller, *Phys. Rev. B* **72**, 224509 (2005).
- [73] M. I. Tsindlekht, G. I. Leviev, V. M. Genkin, I. Felner, Y. B. Paderno, and V. B. Filippov, *Phys. Rev. B* **73**, 104507 (2006).
- [74] N. E. Sluchanko, A. N. Azarevich, A. V. Bogach, S. Y. Gavrilkin, V. V. Glushkov, S. V. Demishev, A. V. Dukhnenko, A. B. Lyashchenko, K. V. Mitsen, and V. B. Filipov, *JETP Lett.* **94**, 642 (2011).
- [75] J.-Y. Ge, V. N. Gladilin, N. E. Sluchanko, A. Lyashenko, V. B. Filipov, J. O. Inekeu, and V. V. Moshchalkov, *New J. Phys.* **19**, 093020 (2017).
- [76] A. K. Geim, S. V. Dubonos, J. G. S. Lok, M. Henini, and J. C. Maan, *Nature (London)* **396**, 144 (1998).
- [77] A. A. Abrikosov, *Fundamentals of the Theory of Metals* (North Holland, Amsterdam, 1988).
- [78] G. Eilenberger, *Phys. Rev.* **153**, 584 (1967).
- [79] N. E. Sluchanko, A. N. Azarevich, M. A. Anisimov, A. V. Bogach, S. Y. Gavrilkin, V. V. Glushkov, S. V. Demishev, A. A. Maksimov, I. I. Tartakovskii, E. V. Filatov *et al.*, *JETP Lett.* **103**, 674 (2016).
- [80] M. A. Anisimov, V. V. Glushkov, A. V. Bogach, S. V. Demishev, N. A. Samarin, S. Y. Gavrilkin, K. V. Mitsen, N. Y. Shitsevalova, A. V. Levchenko, V. B. Filippov *et al.*, *J. Exp. Theor. Phys.* **116**, 760 (2013).
- [81] M. Anisimov, A. Bogach, V. Glushkov, S. Demishev, N. Samarin, S. Gavrilkin, K. Mitsen, N. Shitsevalova, A. Levchenko, V. Filippov *et al.*, *Acta Phys. Pol. A* **126**, 350 (2014).
- [82] V. R. R. Medicherla, S. Patil, R. S. Singh, and K. Maiti, *Appl. Phys. Lett.* **90**, 062507 (2007).
- [83] Y. S. Ponosov and S. V. Strel'tsov, *JETP Lett.* **97**, 447 (2013).
- [84] H. Werheit, V. Filipov, and N. Shitsevalova, *Z. Anorg. Allg. Chem.* **641**, 1835 (2015).

- [85] N. Sluchanko, V. Glushkov, S. Demishev, A. Azarevich, M. Anisimov, A. Bogach, V. Voronov, S. Gavrilkin, K. Mitsen, A. Kuznetsov *et al.*, *Phys. Rev. B* **96**, 144501 (2017).
- [86] E. S. Zhukova, B. P. Gorshunov, G. A. Komandin, L. N. Alyabyeva, A. V. Muratov, Y. A. Aleshchenko, M. A. Anisimov, N. Y. Shitsevalova, S. E. Polovets, V. B. Filipov *et al.*, *Phys. Rev. B* **100**, 104302 (2019).
- [87] N. E. Sluchanko, in *Rare-Earth Borides*, edited by D. S. Inosov (Jenny Stanford Publishing, Singapore, 2021).
- [88] O. N. Khrykina, A. P. Dudka, N. B. Bolotina, N. E. Sluchanko, and N. Y. Shitsevalova, *Solid State Sci.* **107**, 106273 (2020).
- [89] G. M. Kalvius, D. R. Noakes, R. Wäppling, A. Kratzer, E. Schreier, F. Iga, T. Takabatake, and H. Löhneysen, *Phys. B: Condens. Matter* **312**, 210 (2002).
- [90] G. M. Kalvius, D. R. Noakes, N. Marcano, R. Wäppling, F. Iga, and T. Takabatake, *Phys. B: Condens. Matter* **326**, 398 (2003).
- [91] J.-Y. Ge, J. Gutierrez, A. Lyashchenko, V. Filipov, J. Li, and V. V. Moshchalkov, *Phys. Rev. B* **90**, 184511 (2014).
- [92] P. K. Biswas, Ph.D. Thesis, University of Warwick, 2012.
- [93] D. Saint-James, G. Sarma, and E. J. Thomas, in *Type II Superconductivity* (Pergamon Press, Oxford, 1969), p. 264.
- [94] E. J. Nicol and J. P. Carbotte, *Phys. Rev. B* **71**, 054501 (2005).
- [95] P. B. Allen and R. C. Dynes, *Phys. Rev. B* **12**, 905 (1975).
- [96] V. A. Gasparov, in *Boron Rich Solids: Sensors, Ultra High Temperature Ceramics, Thermoelectrics, Armor*, edited by N. Orlovskaya and M. Lugovy (Springer Science+Business Media, New York, 2011), p. 237.
- [97] M. Belogolovskii, I. Felner, and V. Shaternik, in Ref. [96], p. 195.
- [98] J. C. Phillips, *Proc. Natl. Acad. Sci. USA* **107**, 1307 (2010).
- [99] S. Thakur, D. Biswas, N. Sahadev, P. K. Biswas, G. Balakrishnan, and K. Maiti, *J. Appl. Phys.* **114**, 053904 (2013).
- [100] A. A. Golubov, A. Brinkman, O. V. Dolgov, J. Kortus, and O. Jepsen, *Phys. Rev. B* **66**, 054524 (2002).
- [101] M. Zehetmayer, H. W. Weber, and E. Schachinger, *J. Low Temp. Phys.* **133**, 407 (2003).
- [102] M. Zehetmayer, M. Eisterer, J. Jun, S. M. Kazakov, J. Karpinski, A. Wisniewski, and H. W. Weber, *Phys. Rev. B* **66**, 052505 (2002).
- [103] A. V. Sologubenko, J. Jun, S. M. Kazakov, J. Karpinski, and H. R. Ott, *Phys. Rev. B* **65**, 180505 (2002).
- [104] L. Lyard, P. Samuely, P. Szabo, T. Klein, C. Marcenat, L. Paulius, K. H. P. Kim, C. U. Jung, H.-S. Lee, B. Kang *et al.*, *Phys. Rev. B* **66**, 180502 (2002).
- [105] S. Haas and K. Maki, *Phys. Rev. B* **65**, 020502 (2001).
- [106] T. Ma, H. Li, X. Zheng, S. Wang, X. Wang, H. Zhao, S. Han, J. Liu, R. Zhang, P. Zhu, Y.W. Long, J.-G. Cheng, Y. Ma, Y. Zhao, C. Jin, and X. Yu, *Adv. Mater.* **29**, 1 (2016).